J. Fluid Mech. (1998), *vol.* 359, *pp.* 109–142. Printed in the United Kingdom

Effects of external flow on compositional and particle gravity currents

By MARK A. HALLWORTH, ANDREW J. HOGG AND HERBERT E. HUPPERT

Institute of Theoretical Geophysics, Department of Applied Mathematics and Theoretical Physics, University of Cambridge, Silver Street, Cambridge CB3 9EW, UK
e-mail: hallworth@esc.cam.ac.uk, hogg@esc.cam.ac.uk, heh1@esc.cam.ac.uk

(Received 27 June 1997 and in revised form 13 November 1997)

The propagation at high Reynolds number of a heavy, two-dimensional gravity current of given initial volume at the base of a uniform flow is considered. An experimental setup is described for which a known volume of fluid is rapidly introduced halfway down a 9 m channel in which there is a uniform flow of water. The density excess of the released fluid is produced by either dissolving salt or suspending particles in water. The upstream and downstream propagation of the current was measured for different initial salt concentrations, particle sizes and concentrations. A simple box model for the motion of and deposit from the gravity current is constructed. The analytical results obtained compare well with our numerical solutions of one-layer and two-layer models incorporating the appropriate shallow-water equations. Both sets of results are in very good agreement with the experimental data.

1. Introduction

Gravity currents occur whenever fluid of one density flows primarily horizontally into fluid of a different density. (If the flow is primarily vertical it is generally studied as convection.) Gravity currents arise frequently in industrial, laboratory and natural situations. Much of what is known of their motion and particular properties has been nicely summarized by Simpson (1997). The first analysis of the motion of a gravity current was carried out by von Kármán (1940) in response to an enquiry by the American military before World War II concerning the wind speeds that would blow released nerve gas back onto friendly troops. Using the Bernoulli equation for inviscid flow in a manner that was later made rigorous by Benjamin (1968), von Kármán established that if the current intrudes along a horizontal base beneath a very deep, otherwise quiescent fluid, the velocity at the front of the current u_N is related to the depth of the current just behind the head h_N by

$$u_N = Fr(g'h_N)^{1/2}, \tag{1.1}$$

where the Froude number of the flow Fr is constant ($\sqrt{2}$ according to perfect fluid theory, with the incorporation of the Boussinesq approximation) and the reduced gravity

$$g' = (\rho_c - \rho_a)g/\rho_a \tag{1.2}$$

is defined in terms of the gravitational acceleration g and densities ρ_c and ρ_a of the current and ambient respectively.

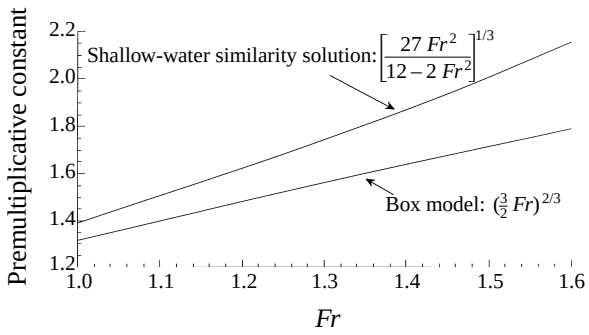

FIGURE 1. Graphical representation of the premultiplicative constants for the shallow-water similarity solution and the box model, given by (1.6), plotted as a function of the Froude number.

Such was the stature of von Kármán that this was hailed as a wonderful result without it being fully appreciated that (1.1) is but one boundary condition between two unknowns and that it says nothing directly about the influence of following or retarding flows in the background ambient. In order to proceed one needs at least to know more about the generation of the gravity current: fixed volume derived from an instantaneous release; fixed flux; or some other alternative. Given this added condition it is possible either to obtain a similarity solution to the governing shallow water equations (Chen 1980; Bonnecaze, Huppert & Lister 1993) or to construct a simple 'box' model of the flow which assumes that there is no horizontal variation of properties within the flow and manipulates the two given conditions to derive a relationship for the rate of propagation and (horizontally uniform) depth of the current as functions of time. For a two-dimensional, fixed volume, instantaneous release the latter approach is achieved by writing (1.1) as

$$\dot{l} = Fr(g'h)^{1/2}, \tag{1.3}$$

where $l(t)$ is the length of the current, and the constraint of fixed volume (under the assumption of zero entrainment) as

$$lh = A, \tag{1.4}$$

where A is the constant volume per unit width, or two-dimensional area. Substituting (1.4) into (1.3) and integrating the result along with the boundary condition

$$l = 0 \quad (t = 0), \tag{1.5}$$

we obtain

$$l = (\tfrac{3}{2}Fr)^{2/3}(g'A)^{1/3}t^{2/3}. \tag{1.6}$$

The similarity solution to the shallow-water equations is identical to (1.6) (as will be further illustrated in § 4.2) except that the pre-multiplicative constant

$$(\tfrac{3}{2}Fr)^{2/3} \quad \text{is replaced by} \quad \left[\frac{27Fr^2}{12-2Fr^2}\right]^{1/3}.$$

The difference between these two expressions is small for $1 \leqslant Fr \leqslant 1.6$, as is shown graphically in figure 1. In both cases the area appears only in the product $g'A$, the total buoyancy, which remains constant, independent of entrainment of ambient fluid. (For a discussion of the effects of entrainment see Hallworth *et al.* 1996.)

Gravity currents driven by the excess buoyancy arising from the presence of

suspended particles are fundamentally different from homogeneous single-phase flows, because the heavy particles continually settle out of the flow. The concentration of particles and consequently the buoyancy force thus changes with time and position. In this situation the appropriate shallow water equations do not admit a similarity solution and have to be solved numerically after the introduction of the volume concentration of particles ϕ (Bonnecaze *et al.* 1993). A simple box-model approach commences by writing the density of the current ρ_c as

$$\rho_c = \rho_p \phi + \rho_a (1 - \phi),$$

where ρ_p is the density of the particles and the density of the interstitial fluid has been assumed equal to that of the ambient. The reduced gravity of the current g' is then expressed in terms of the reduced gravity of the particles g'_p as

$$g' = g'_p \phi, \tag{1.7}$$

where

$$g'_p = g(\rho_p - \rho_a)/\rho_a. \tag{1.8}$$

The front condition then becomes

$$\dot{l} = Fr(g'_p \phi h)^{1/2}, \tag{1.9}$$

while following the arguments of Pantin (1979), Martin & Nokes (1988), Bonnecaze *et al.* (1993) and others on the settling of small particles in a well-mixed turbulent flow, the evolution of particle concentration in the flow is governed by

$$\dot{\phi} = -V_s \phi / h, \tag{1.10}$$

where V_s is the Stokes free-fall velocity given by $2g'_p a^2/(9\nu)$, ν is the kinematic viscosity and a is a representative length scale of the particle – the radius if it is spherical; the radius of the enveloping sphere in most situations if it is aspherical (Batchelor 1970). To the three equations (1.4), (1.9) and (1.10) for the three unknowns $l(t), h(t), \phi(t)$ are added the two initial conditions

$$l = 0, \quad \phi = \phi_0 \quad (t = 0). \tag{1.11 a, b}$$

Dividing (1.10) by (1.9) and using (1.4) to eliminate h, we obtain

$$\frac{\mathrm{d}\phi}{\mathrm{d}l} = -\lambda l^{3/2} \phi^{1/2} \tag{1.12}$$

with (1.11) expressed as

$$\phi = \phi_0 \quad (l = 0), \tag{1.13}$$

where

$$\lambda = V_s / (Fr^2 g'_p A^3)^{1/2}. \tag{1.14}$$

Equation (1.12) with initial condition (1.13) has solution

$$\phi^{1/2} = \phi_0^{1/2} - \tfrac{1}{5} \lambda l^{5/2}, \tag{1.15}$$

from which it is immediately seen that the current ceases ($\phi = 0$) at

$$l_\infty = (5\phi_0^{1/2}/\lambda)^{2/5}. \tag{1.16}$$

Introducing non-dimensional variables $\Phi = \phi/\phi_0$ and $\xi = l/l_\infty$, we can rewrite

(1.15) as

$$\Phi = (1 - \xi^{5/2})^2. \tag{1.17}$$

Substituting (1.4) and (1.17) into (1.9) and using the initial condition (1.11*a*), we obtain

$$\tau = \int_0^{\xi} \frac{s^{1/2}\mathrm{d}s}{1 - s^{5/2}} \equiv \mathscr{F}(\xi) \tag{1.18 a,b}$$

in terms of the dimensionless time τ given by

$$\tau = Fr(g_p' A\phi_0)^{1/2} l_\infty^{-3/2} t. \tag{1.19}$$

These relationships, using a Froude number of 1.19 (Huppert & Simpson 1980), are plotted in figure 2(*a*) along with some confirmatory experimental data for the length of the current as a function of time taken from Bonnecaze *et al.* (1993) and Dade & Huppert (1994). The box model overestimates the value of l_∞ given in (1.16) by a factor of approximately 1.6, as noted by Bonnecaze *et al.* (1995). Hence all the experimental lengths were divided by 1.6 before being plotted in figure 2(*a*). We see that the proposed scaling collapses all the data well and that the agreement with the theoretical prediction is good. The difference between the simple box model and the experimental data is probably due to the fact that motions in the upper layer of the experiments, neglected in the box model, play a small role, as is discussed further in § 4.4, following the results of Bonnecaze *et al.* (1993) (see particularly their figure 12).

In order to evaluate the resulting deposit distribution, we argue that in time δt, a mass per unit width $\delta M = -\rho_p A \delta\phi$ is deposited uniformly over a length l to lead to a deposit density

$$\delta\eta = -\rho_p A \delta\phi / l. \tag{1.20}$$

Thus the total deposit density (of dimensions ML^{-2}) after the flow has ceased is given by

$$\eta = -\rho_p A \int_l^{l_\infty} s^{-1} \frac{\mathrm{d}\phi}{\mathrm{d}s} \mathrm{d}s. \tag{1.21}$$

Differentiating (1.17), substituting the result into (1.21) and carrying out the integration, we find that

$$\eta = \frac{25\phi_0 \rho_p A}{12 l_\infty} (1 - \tfrac{8}{5}\xi^{3/2} + \tfrac{3}{5}\xi^4) \tag{1.22}$$

which is graphed and compared with experimental data in figure 2(*b*). The agreement between the data and the theory is again seen to be good, except near the back of the channel where the particles seem to be swept downstream more than theory would suggest.

The above results are for monodisperse particles with a single fall speed V_s. Bonnecaze, Huppert & Lister (1996) considered, both theoretically and experimentally, the deposit generated when the current is driven by a polydisperse distribution of particles. Using dimensional analysis on the governing shallow water equations and their initial conditions, they argued that the total deposit density due to an initial distribution of N particle sizes, each with Stokes free-fall speed V_i and initial volume concentration ϕ_{i0} ($i = 1, 2, \ldots, N$) could be written in terms of a shape function $W(s)$ as

$$\eta(x) = \rho_p A \sum_{i=1}^{N} \phi_{i0} \gamma_i W(\gamma_i x), \tag{1.23}$$

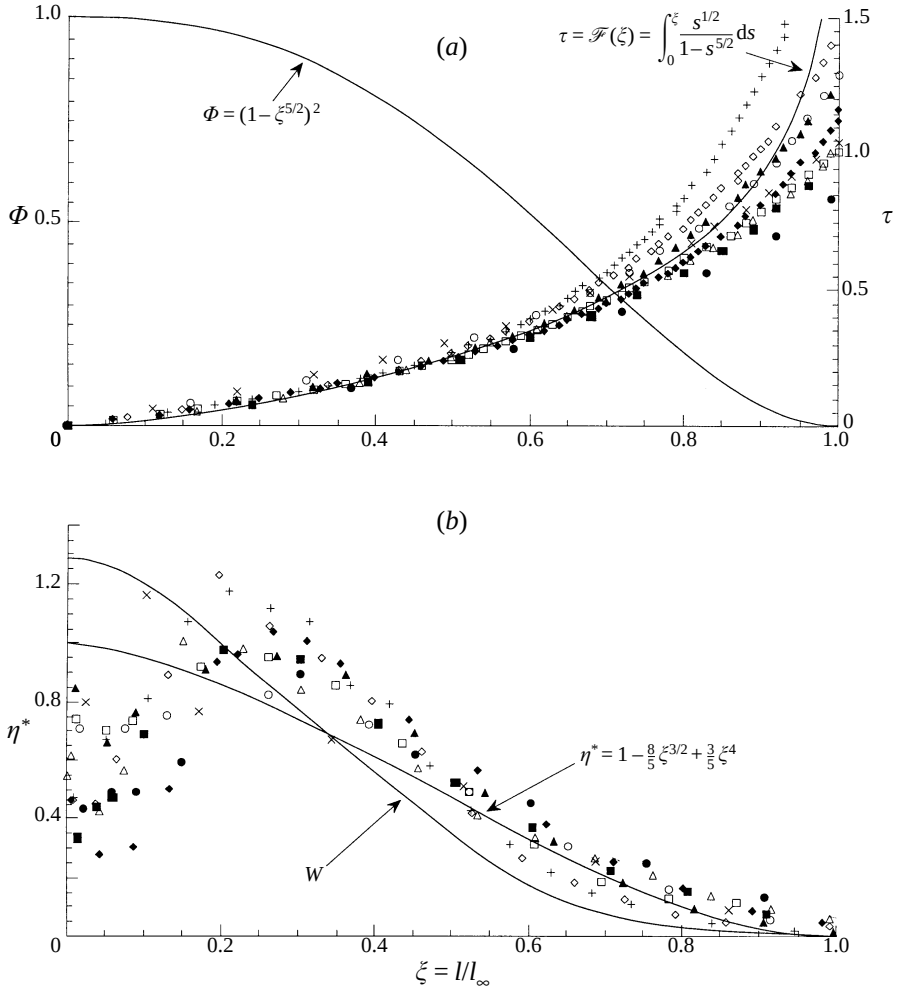

FIGURE 2. Data and non-dimensional box-model solutions for particle-driven gravity currents released at one end of a channel containing quiescent ambient fluid. The data points are from the experiments of Bonnecaze *et al.* (1993) and Dade & Huppert (1994) covering a large range of different initial conditions. (*a*) The non-dimensional volume fraction Φ (equation (1.17)) and time τ (equation (1.18)), as functions of the non-dimensional current length ξ. (*b*) The non-dimensional deposit density η^*, where $\eta^* = 12l_\infty\eta/25\phi_0\rho_p A$ from equation (1.22), plotted as a function of non-dimensional current length ξ. The curve denoted by W is the appropriately non-dimensional empirical relationship suggested by Bonnecaze *et al.* (1996) and expressed by equation (1.25).

where

$$\gamma_i = [V_i^2/(g_o' A^3)]^{1/5} \tag{1.24a}$$

and

$$g_0' = g_p' \sum_{i=1}^{N} \phi_{i0}. \tag{1.24b}$$

From their numerical solutions of the shallow water equations, they suggested that a convenient and accurate empirical representation of $W(\bar{x})$ (which conserves mass) is

given by

$$W(\bar{x}) = 0.820/(1 + 0.683\bar{x}^2 + 0.017\bar{x}^8), \tag{1.25}$$

which appropriately non-dimensionalized and incorporating the factor of 1.6 described above, is also sketched in figure 2(*b*). The agreement between the two theoretical relationships is seen to be good.

The purpose of this paper is to ascertain how all these results are influenced by an opposing or following uniform flow. Some work has been performed on the influence of such flows on a compositional current (although in a different release configuration) by Simpson & Britter (1980), Xu (1992) and Xu & Moncrieff (1994), as will be described in more detail below. No previous paper known to us, however, has considered the influence of such flows on a particle-driven gravity current.

In the next section we describe the procedure and results of several experiments in which a fixed volume of relatively dense fluid was suddenly released into the centre of an open channel through which a uniform flow of water was maintained. The density excess of the released fluid was produced using either salt solutions or low-concentration suspensions of small heavy particles, and resulted in gravity currents which propagated along the channel floor both downstream (with the ambient flow) and upstream (against the ambient flow).

A simple box model is presented in § 3 which leads to results which are in very good agreement with the experimental data. In particular, we show that for compositional currents: the maximum distance upstream that the current can propagate scales with $g'A/U^2$, where U is the (downstream) velocity of the ambient; the total length of the current increases as $t^{2/3}$; and the centroid of the current propagates downstream at 0.6 times that of the ambient velocity. For a particle-driven gravity current we find that: the total length of the current is given by $2^{2/5}l_\infty$, independent of U; and the maximum upstream penetration scales with l_∞ and is a function of a single additional parameter $\Lambda \propto (UA/l_\infty^2 V_s)$, which incorporates the ratio of the ambient to the sedimentation velocity. A rigorous numerical solution of the shallow-water equations is presented in § 4, which reproduces the results obtained by the box model, except for a few slight quantitative differences. We are able by this numerical approach, however, to discuss some phenomena due to the influence of the gravity current on motions in the upper layer. In particular, our numerical solutions are able to highlight differences between a two-layer and a one-layer flow model. A few applications of our results are discussed in the final section.

2. Experiments

2.1. *Experimental set-up*

The experimental apparatus used is shown schematically in figure 3. A 9.4 m long Perspex channel having a rectangular cross-section 26 cm wide and 50 cm high was filled with water to a depth H of 28.7 cm. A uniform ambient flow was established by pumping the water at a fixed rate in a continuous loop via a hose connecting inlet and outlet diffuser boxes situated at either end of the channel, thereby giving a working flow section of 8.4 m. Each diffuser box comprised a flared section packed with 1cm diameter plastic balls and a horizontally aligned honeycomb section, designed to introduce and withdraw the flow evenly across the whole cross-sectional area of the channel. Profiles of the flow velocity as a function of depth were measured at several distances along the medial plane of the working section using a Sontek acoustic Doppler velocimeter (Lane *et al.* 1997). This non-intrusive device focuses an

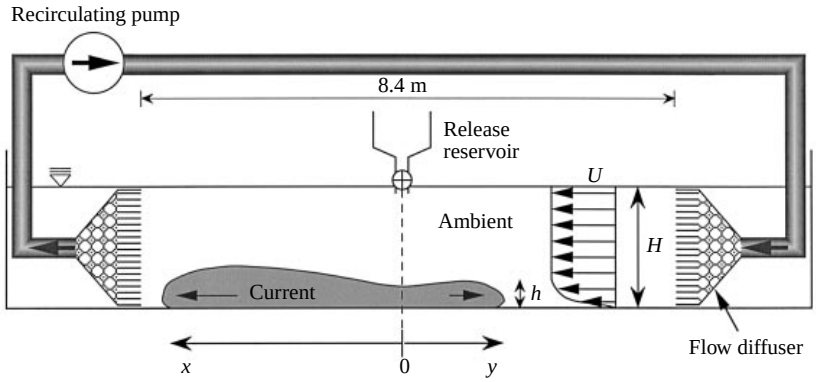

FIGURE 3. Schematic diagram of the experimental apparatus (not to scale).

acoustic beam on a 0.5 cm^3 fluid sample volume and digitally translates the reflected signal into three mutually perpendicular velocity components, which we orientated to coincide with the major axes of the channel. Both the vertical and horizontal cross-stream velocity components were negligible. The horizontal downstream velocity components at various positions are presented as velocity profiles in figure 4(*a*). Each profile displays a fairly uniform velocity averaging 2.9 $cm\,s^{-1}$ in the interior of the flow which reduces in value to zero at the channel floor through a lower boundary layer, approximately 2 cm thick. A reduction in flow velocity is also apparent as the free surface is approached. Integration of these flow profiles yielded an average volumetric flux of 1850 $cm^3\,s^{-1}$, which corresponds to a Reynolds number of approximately 7000. The measured flux was found to be in good agreement with independent measurements of the pump throughput, as shown on figure 4(*b*).

The conventional lock-release method of initiating fixed-volume gravity currents into a stationary ambient fluid was impossible to achieve in the present situation without severely disrupting the ambient flow. An alternative release mechanism was therefore designed whereby a fixed volume of dense fluid, initially held in a reservoir above the mid-point of the channel, was allowed to drain rapidly (in less than 1 s) into the flow stream through a 3 cm diameter tube positioned just beneath the free surface. The emergent jet of dense fluid inevitably entrained a significant volume of ambient fluid during its descent and subsequent lateral deflection upon impinging on the solid channel floor. A somewhat similar situation, of compositional density currents initiated from a continual flux of downward momentum, was investigated by Linden & Simpson (1990).

Testing of our release mechanism in quiescent ambient conditions indicated that the jet split equally and extended roughly 30 cm either side of the central release position before buoyancy forces began to dominate the motion. Entrainment of ambient fluid during the early momentum-dominated phase was measured to cause a dilution of the released fluid by a factor of approximately 20. This estimate was achieved by trapping a released current between vertical barriers, positioned either 50 or 100 cm on either side of the entry point. When confined in this manner, the dense flow eventually settled to form a layer of constant composition. By measuring the height of this layer, its volume could be calculated and compared with the initial volume. In each case our measurements indicated that the released fluid was diluted by a factor of 20 ± 2 through entrainment of ambient fluid over the momentum-dominated jet entry length.

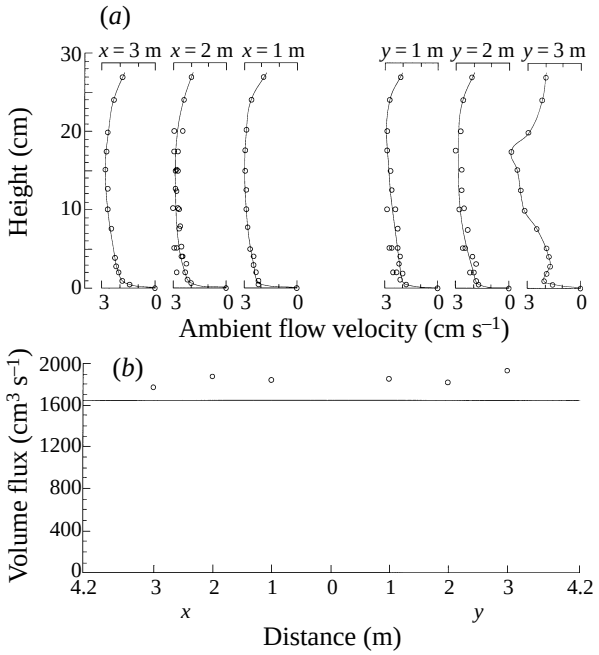

FIGURE 4. (*a*) Profiles of the horizontal downstream ambient fluid velocity as a function of depth, measured by acoustic Doppler velocimetry at various distances either side of the release position along the medial plane of the flow channel (in the absence of gravity currents). The structure in the profile at $y = 3$ m is due to the proximity of this section to the input diffuser box. (*b*) The volume flux of ambient fluid as a function of distance from the release position, calculated by multiplying the width of the channel by the integrated value of the velocity profiles shown in (*a*) over the total depth. The solid line represents the independently measured pump flow rate. The integrated flow values are slightly in excess of the estimated overall flux because no account was taken of the sidewall boundary layers in the determination of the integrated flux.

In this study we focus on the dynamics of gravity currents that are controlled by a balance between inertial and buoyancy forces. However, because of the elevated reservoir used to initiate the current, it is possible that the flow may be strongly influenced by the initial momentum imparted to it. We may assess the influence of the initial specific momentum flux as follows. The fluid leaves the reservoir at a velocity approximately given by

$$u_e = (2gH_r)^{1/2}, \tag{2.1}$$

where H_r is the elevation of the base of the reservoir above the free surface. Therefore, the initial specific momentum of the fluid is approximately given by

$$M = Vu_e, \tag{2.2}$$

where V is the total volume of fluid discharged. The (conserved) specific buoyancy of the fluid is given by

$$B = Vg'. \tag{2.3}$$

Hence we may estimate a jet entry length as

$$L_e = (M^2/B)^{1/4}. \tag{2.4}$$

For distances much less than this entry length, the flow is dominated by its initial momentum, whereas at distances sufficiently large compared to L_e the flow is domi-

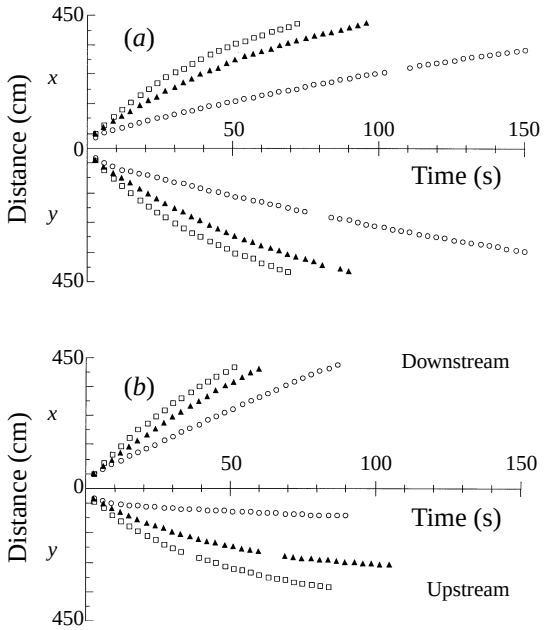

FIGURE 5. Lengths as a function of time for various compositional currents of fixed volume released at the mid-point of a channel containing (*a*) quiescent ambient fluid and (*b*) ambient fluid with a mean downstream velocity of 2.6 cm s^{-1}. Results are presented in each case for initial released volumes of 2 l of water containing 50 g (○), 200 g (▲) and 400 g (□) of dissolved salt.

nated by buoyancy. Substituting the experimental values of this study into (2.1)–(2.4), we find that $L_e = 30$ cm which is in accord with indications from our experimental observations. Therefore, we conclude that during the descent through the ambient fluid, the flow was predominantly controlled by momentum, whereas once the gravity current along the lower boundary had been initiated, the flow was dominated by buoyancy forces.

Measurements were made of the horizontal distance to the front of the current from the release point as functions of time in both the downstream (x) and upstream (y) directions by marking the position of the nose of the current at 3 s intervals. From these measurements and observations of the thickness of the currents we estimate that their Reynolds numbers were initially in excess of a thousand but necessarily decreased as the flows evolved. We are confident that the measurements we report are for flows dominated by high-Reynolds-number effects.

In the case of particle-driven gravity currents, the final distribution of sedimented particles was measured by recovering the mass of particles within a 5 cm wide strip across the width of the tank at various distances from the release point.

2.2. *Compositional currents*

Compositional currents of different initial densities were generated by releasing 2 l of water containing 50, 200 and 400 g of dissolved salt into the ambient flow, resulting in initial values of g' of 17.1, 64.4 and 121 cm s^{-2} respectively ($g'A$ = 1330, 4990 and 9380 cm^3 s^{-2}). Solutions of each concentration were also released into a quiescent ambient for comparison. Almost all experiments were repeated at least once and were found to show excellent reproducibility. Measurements of the position of the foremost point of the currents in both the x- and y-directions as functions of time

are presented in figure 5. The currents released into a quiescent ambient fluid spread symmetrically away from the release point in both directions, and adopted the typical gravity current profile of a lobate billowing head advancing before a thinner tail region. A predictable increase in velocity was observed with increasing initial salt concentration. By contrast, equivalent currents released into a uniform ambient flow advanced both upstream and downstream, but were markedly asymmetrical. In the downstream (x) direction, the current was noticeably thicker than its counterpart in a static environment, and propagated with an increased velocity. As distance from the release point increased, the velocity of the current gradually decreased to a value approaching 0.6 times the mean ambient velocity (see § 3.1). In the upstream (y) direction, the current was significantly retarded by the opposing ambient flow, and eventually came to rest. Prior to final arrest, the current profile was observed to undergo a transition from the typical head and tail into a much thinner wedge shape within the lower boundary layer. Once in this form, dense fluid was continually stripped away from the upper surface of the arrested wedge by the action of interfacial eddies.

2.3. *Particle currents*

The particle-driven gravity currents were generated by releasing well-mixed suspensions of silicon carbide particles in water. These particles are fairly monodisperse, non-cohesive and have a density $\rho_p = 3.217\,\mathrm{g\,cm^{-3}}$. As a precaution, a small amount of Calgon was added to the suspension to prevent particle agglomeration. Three different particle sizes were used, with mean diameters of 23, 37 and 53 μm. Details of the size distribution within each grade are reported in Huppert *et al.* (1991).

For each particle size, experiments were run with four different initial particle masses of 50, 100, 200 and 400 g suspended in 2 l of water, giving values for ϕ_0, the initial volume fraction, of 0.0077, 0.015, 0.030 and 0.059; and g' values of 16.7, 33.3, 65.5 and $127\,\mathrm{cm\,s^{-2}}$, respectively. Upon release, the particle-driven gravity currents propagated with decreasing velocity in both the x- and y-directions while simultaneously depositing a sediment layer over the channel floor until all the particles had settled out, whereupon the current ceased to exist.

Measurements of the position of the foremost point of the currents in both the x- and y-directions as functions of time for release into both a quiescent ambient and a uniform ambient flow, are displayed in figure 6. Velocities of the current at any point achieved by each flow were observed to increase monotonically with increasing initial mass of suspended sediment, and the current attained progressively longer maximum distances from the release point with decreasing particle diameter. Currents released into a quiescent ambient spread symmetrically about the release point, whereas those released into an ambient flow were markedly elongated in the downstream direction. The development of an arrested wedge of dense fluid in the upstream direction was not as noticeable as that seen in the compositional currents, since particles quickly sedimented from thinned flows in the slow moving lower boundary layer of the opposing stream.

Once all the particles had settled out, the final length of the deposited layer was recorded, and its mass distribution measured by vacuuming up the sediment using a siphon tube within a 5 cm $\times$25 cm rectangular pastry cutter placed over the layer at specific intervals. The mixture was collected in a beaker, the water decanted and the particles dried and weighed to determine the mass of deposit per unit area. Depositional profiles for selected experiments are graphed in figure 7. As a check on the sampling method, the total mass of sediment was recovered by integrating the

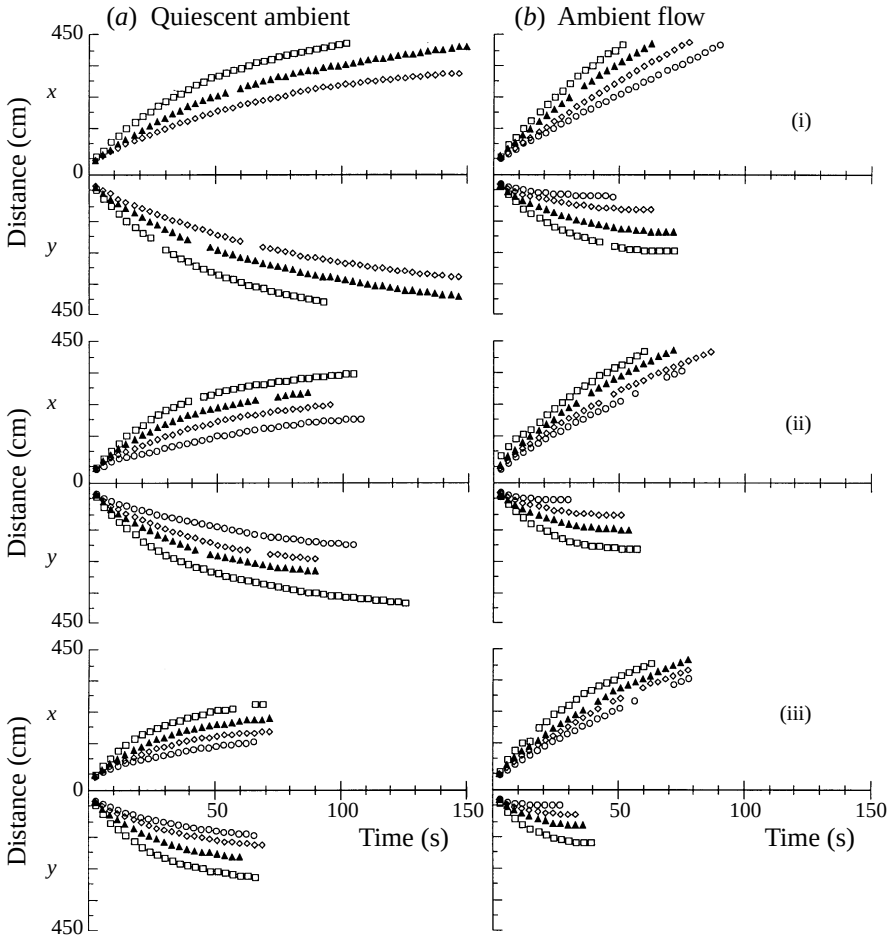

FIGURE 6. Lengths as a function of time for various particle-driven gravity currents of fixed volume, released at the mid-point of a channel containing (*a*) quiescent ambient fluid, and (*b*) ambient fluid with a mean downstream velocity of 2.6 cm s^{-1}. Results are presented in each case for three mean particle diameters of (i) 23 μm, (ii) 37 μm and (iii) 53 μm, at four different initial masses of sediment, 50 g (○), 100 g (◇), 200 g (▲) and 400 g (□), suspended in 21 of water.

measured deposition profile and was generally found to be within 1% of the initial value.

These experimental data can be drawn together using the analytical models to be developed in the next sections.

3. Box model

A box-model representation of the intrusion can be obtained using the approach outlined in the Introduction, on the assumption that at all times the salt concentration, or the particle distribution, in the current and its height are uniform in the horizontal direction.

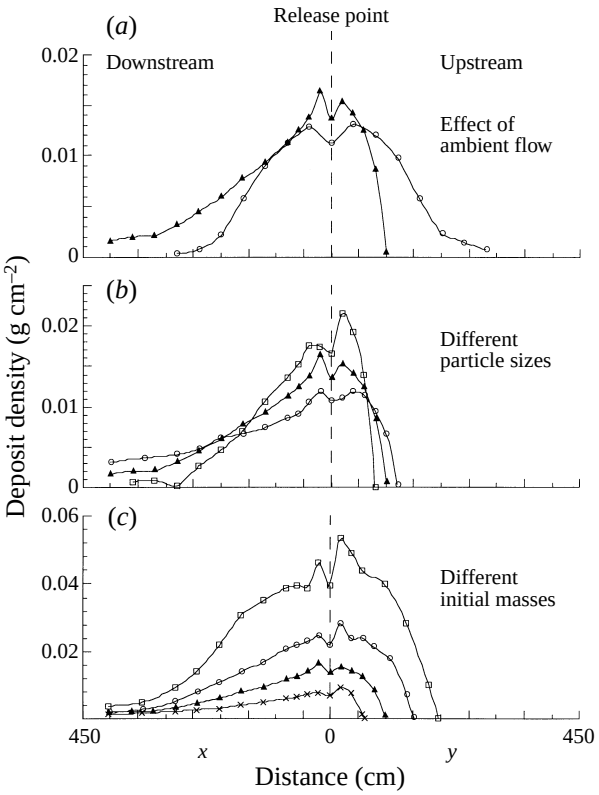

FIGURE 7. Individual data and interpolated smooth curves for the deposit density of sedimented particles following the passage of various particle-driven gravity currents. Each graph presents the mass per unit area as a function of distance from the release point in both directions. (*a*) Two currents each initially containing 100 g of 37 μm particles suspended in 21 of water, released into a quiescent ambient (○) and an ambient flow (▲). (*b*) Three currents each initially containing 100 g of particles of mean diameters 23 μm (○), 37 μm (▲) and 53 μm (□) suspended in 21 of water and released into an ambient flow. (*c*) Four currents with different initial masses of 50 g (×), 100 g (▲), 200 g (○) and 400 g (□) of 37 μm particles initially suspended in 21 of water and released into an ambient flow.

3.1. *Compositional currents*

The condition of conservation of volume becomes

$$l \equiv x + y = A/h \tag{3.1}$$

while the *two* front conditions become

$$\dot{x} - U = Fr(g'h)^{1/2} \tag{3.2a}$$

and

$$\dot{y} + U = Fr(g'h)^{1/2}, \tag{3.2b}$$

where U is the mean velocity in the x-direction, experienced by the current. As will be discussed below, this velocity is equal to 0.6 times that of the mean flow. In this analysis and that of § 3.2 we use a Froude number of 1.19 (Huppert & Simpson 1980). For the purposes of this simple model we have neglected the variation of the Froude number with the relative magnitude of the mean flow. Some studies have indicated that this may be a significant consideration (Simpson & Britter 1980; Xu

1992; and see the appendix). However, from these experiments we are unable to assess the magnitude of these variations.

Substituting (3.1) into (3.2), adding and subtracting the resulting two equations and solving these subject to

$$x = y = 0 \quad (t = 0), \tag{3.3}$$

leads to solutions

$$x = Ut + \gamma t^{2/3}, \quad y = -Ut + \gamma t^{2/3}, \tag{3.4 a, b}$$

where

$$\gamma = \tfrac{1}{2}(3Fr)^{2/3}(g'A)^{1/3} \tag{3.5}$$

(cf (1.6)). From (3.4*b*) we predict that the maximum distance upstream that the current propagates is given by $\frac{1}{6}Fr^2(g'A/U^2)$, which except for the pre-multiplicative constant can be simply obtained by dimensional analysis.

Inspection of (3.4) indicates that there is a timescale

$$\tau_c = (\gamma/U)^3, \tag{3.6}$$

which is around 200 s for our experiments. For times less than τ_c the current propagates mainly due to buoyancy, and the effects of the external flow make a smaller contribution; for $t > \tau_c$ external flow effects are more important than the buoyancy. Our experiments were conducted for a duration of around 60 s, beyond which the gravity current became too thin and weak to be distinguished against the background flow. (After this time the Reynolds number of the current was also too small for the above theory to be appropriate.) It was thus impossible for us to test robustly both of the terms of (3.4) (in the form written).

It is therefore worthwhile concentrating on the alternative representations

$$l \equiv x + y = 2\gamma t^{2/3}, \quad z \equiv x - y = 2Ut, \tag{3.7 a, b}$$

which evaluate the evolution of the length and twice the position of the centre of the current. Introducing the lengthscale

$$l_c = \gamma^3/U^2 \tag{3.8}$$

and the non-dimensional variables

$$L_c = l/l_c, \quad Z_c = (x - y)/l_c \quad \text{and} \quad T_c = t/\tau_c, \tag{3.9 a–c}$$

we plot all our experimental data in figure 8 and compare these to our theoretical predictions

$$L_c = 2T_c^{2/3} \quad \text{and} \quad Z_c = 2T_c. \tag{3.10 a, b}$$

We note that in these non-dimensionalizations the velocity U is taken to be 0.6 of the mean ambient flow. That a gravity current only experiences 0.6 of the mean flow has been suggested previously by Simpson & Britter (1980) and in this study we find further extremely strong experimental evidence of this fact (see § 3.2). We noted in § 2.1 that on initial entry to the ambient from the elevated reservoir, the relatively dense fluid undergoes rapid dilution. However in the theoretical description of compositional currents, the initial area, A, only occurs in the total buoyancy, $g'A$, and this is conserved under mixing.

The agreement between the theoretical predictions and the experimental data is good and suggests that the relationships (3.4) for the upstream and downstream

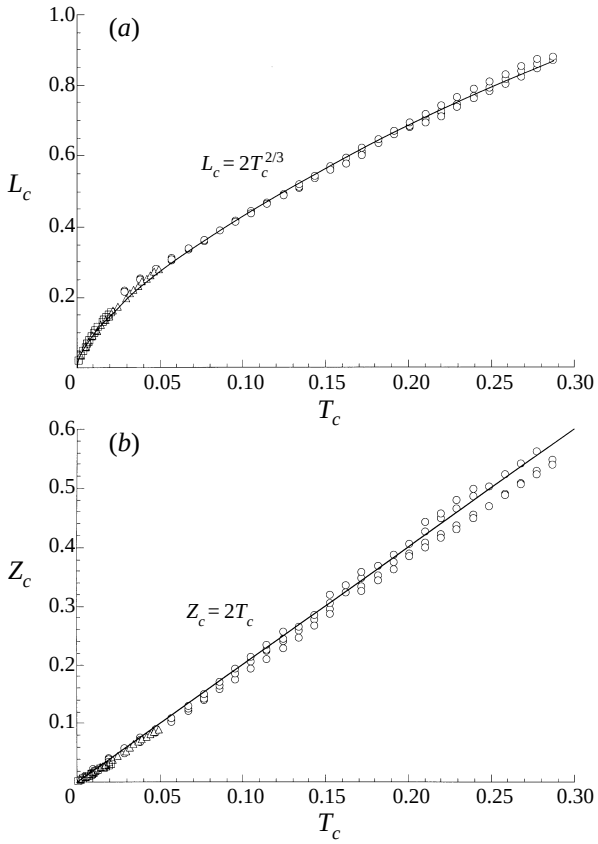

FIGURE 8. (*a*) Non-dimensional length L_c, and (*b*) non-dimensional position of the centroid Z_c, plotted against non-dimensional time T_c, for compositional currents of 50 g (○), 200 g (▲) and 400 g (□) of salt dissolved in 21 of water, released into an ambient flow. The theoretical predictions are shown as solid lines.

position of the current can be used with confidence (beyond the limits for which we have confirmed them). We note that (3.10) indicates that the total length of the current increases as the two-thirds power of the time while the centre of the current propagates downstream at 0.6 times that of the ambient velocity.

3.2. *Particle currents*

In order to develop a box model for the propagation of a monodisperse particle current (3.2) needs to be altered along the lines explained in § 2 to read

$$\dot{x} - U = Fr(g_p' \phi h)^{1/2}, \quad \dot{y} + U = Fr(g_p' \phi h)^{1/2}. \tag{3.11 a, b}$$

The system that requires solution is then (1.10), (3.1) and (3.11) along with the initial conditions (1.11). Using the approach and non-dimensionalizations outlined in §§ 2 and 3.1, we obtain the relationships

$$\Phi = (1 - L^{5/2})^2, \tag{3.12a}$$

$$T = \int_0^L \frac{s^{1/2}\,\mathrm{d}s}{1 - s^{5/2}} \equiv \mathscr{F}(L), \tag{3.12b}$$

$$\bar{z} = \Lambda T, \tag{3.12c}$$

where the non-dimensional variables

$$L = l/l_p, \quad \bar{z} = (x - y)/l_p \quad \text{and} \quad T = t/\tau_p \tag{3.13 a–c}$$

have been defined in terms of the length- and timescales

$$l_p = \left[\frac{10Fr(g'_p\phi_0 A^3)^{1/2}}{V_s}\right]^{2/5} \equiv 2^{2/5} l_\infty \quad \text{and} \quad \tau_p = \frac{5A}{l_p V_s} \tag{3.14 a–c}$$

and the single non-dimensional parameter

$$\Lambda = \frac{10UA}{l_p^2 V_s}. \tag{3.14 d}$$

In contrast to the compositional situation, the current ceases ($\phi = 0$) when $l = l_p$, a value that is (surprisingly) independent of the ambient flow speed, though we see from (3.12*b*) that this length takes (theoretically) an infinite time to achieve. The magnitude of Λ represents the influence of the mean flow on the runout of the gravity current and is proportional to the ratio of the mean flow to the settling velocity of the particles. More precisely, if we re-write A as the product of the runout length l_p and the height of the fluid layer when this length is attained, $A = h_p l_p$, then the parameter Λ may be seen to represent the ratio of the horizontal flux of fluid, Uh_p, to the vertical settling flux of particles, $V_s l_p$. When the settling flux is large compared to the flux of the mean flow (and thus Λ is much less than unity), the evolution of the gravity current is only weakly affected by the motion of the ambient. Conversely, when Λ is much greater than unity, the gravity current is strongly influenced by the mean flow.

In the calculation of the length- and timescales, (3.14*a*, *c*), the initial area A occurs separately from the initial total buoyancy $g'_p A$. This is in contrast to theoretical descriptions of compositional currents and implies that the initial dilution of the particle-laden fluid on entry to the ambient is an important effect. In the following calculations, we use the measured dilution factor of 20 (see § 2.1). We plot in figure 9 the theoretical curves (3.12*b*, *c*) and the experimental data, non-dimensionalized according to the scaling suggested by the box model. We note that the non-dimensionalization collapses the experimental data and that there is very good agreement with the theoretical predictions. The relationship (3.12*c*) suggests that the position of the centroid should depend linearly on ΛT. However as noted in § 3.1, we are uncertain as to the exact value of U to use in the definition of Λ, although previous studies (Simpson & Britter 1980) have indicated that $U = 0.6\overline{U}$, where $\overline{U}$ is the mean velocity in the channel. Figure 9(*b*) presents experimental data on the position of the centroid against $\Lambda T/U$. From the gradient of the fitted curve we find that $U = 1.8\,\mathrm{m\,s^{-1}}$ which corresponds to $U = 0.62\overline{U}$.

The distribution of the deposit arising from these particle-driven gravity currents may also be calculated from the box-model analysis. We assume that the particles sediment out of the current uniformly along its length. When there is no ambient flow, the gravity current propagates symmetrically in the upstream and downstream directions until it attains the maximum length (l_p). In contrast, when there is an ambient flow, the centroid of the current is advected downstream (c.f. (3.12*c*)). Thus the resulting deposit is asymmetric about the initiation line of the two-dimensional current and may, in fact, extend over a considerable distance downstream. (In terms of the box model, the deposit may extend infinitely far downstream because the

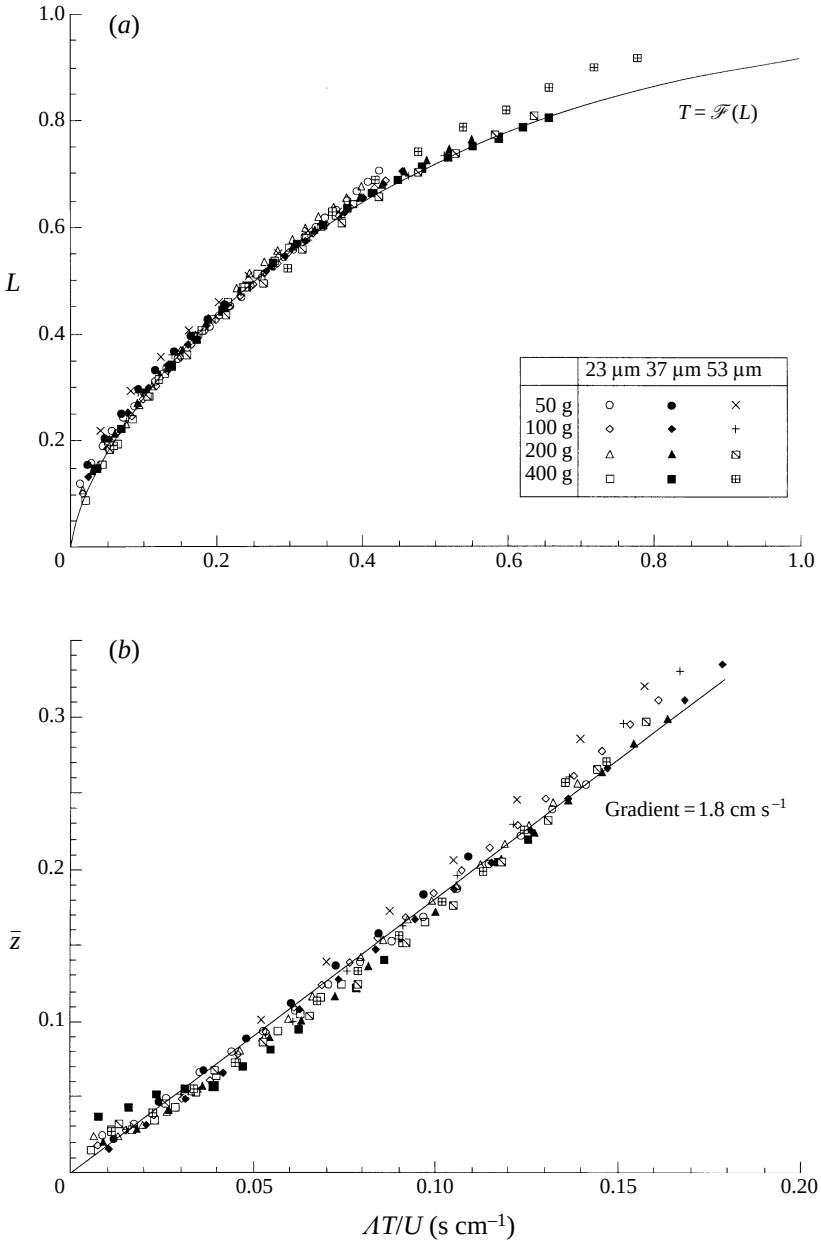

FIGURE 9. (*a*) Non-dimensional length L, plotted against non-dimensional time T, and (*b*) non-dimensional position of centroid $\bar{z}$, plotted against $\Lambda T/U$, for particle currents with various masses and sizes of particles (given by legend) initially suspended in 21 of water, released into an ambient flow. The solid curve in (*a*) is the theoretical relationship given by (3.12*b*). The solid curve in (*b*) is the best-fit straight line through all the data, the gradient of which determines U.

maximum length of the current is only attained after an infinite time. In practice, of course, viscous forces eventually influence the evolution of the flow at which time this model, which is based upon a inertial–buoyancy balance, becomes invalid.) The deposit, expressed as the integrated mass flux per unit area delivered to the bottom

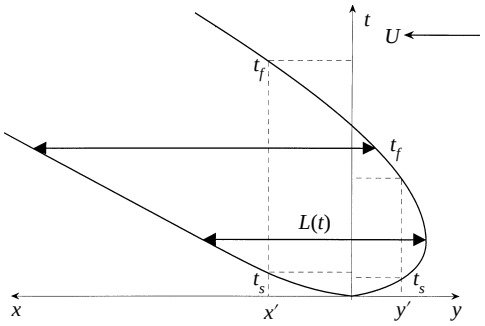

FIGURE 10. Schematic diagram depicting the position of the upstream and downstream fronts as functions of time, showing the progressive increase in the length $L(t)$ of the current with time. At a given upstream position, y', deposition of particles commences when the front of the upstream current first passes at time t_s, and ceases when this front is swept back downstream at time t_f. At a given downstream position, x', deposition of particles starts when the front of the downstream current first passes, and finishes when the upstream front is swept back downstream.

while the current is overhead, is given by

$$\eta(x) = \rho_p V_s \int_{t_s}^{t_f} \phi \, \mathrm{d}t, \tag{3.15}$$

where the limits of this integral correspond to the times at which deposition starts and finishes, denoted by t_s and t_f, respectively. We reiterate that a box model of the gravity current is being used in which there is uniform sedimentation along its entire length. Furthermore the length of the box is increasing whilst its centroid is being advected downstream (as depicted in figure 10). Therefore at a particular location, deposition starts when a front of the current first passes and ceases when the rear of the current is swept by. Substituting (3.12*a*, *b*) into (3.15), we obtain the implicit relationship

$$\eta(x) = \frac{5\phi_0 \rho_p A}{l_p} \left[2L^{3/2}/3 - L^4/4\right]_{L_s}^{L_f}, \tag{3.16}$$

where L_s and L_f are the values of the dimensionless length, L, at non-dimensional times of T_s and T_f, which correspond to the dimensional times t_s and t_f. These are obtained for $x > 0$ by rearranging (3.13) to read

$$L_s = 2x/l_p - \bar{z}, \quad L_f = -2x/l_p + \bar{z}, \tag{3.17 *a*, *b*}$$

while for $x < 0$, the equation

$$L = -2x/l_p + \bar{z} \tag{3.18}$$

has two solutions; we denote the smaller by T_s and the larger by T_f.

We plot some illustrative profiles of the deposit as a function of position for a range of values of Λ in figure 11. As noted above, when there is no ambient flow, $U = \Lambda = 0$, the deposit distribution is symmetric about the point at which the suspension of particles is released. However, as the magnitude of the ambient flow increases relative to the settling velocity of the particles, the profiles become more asymmetric. We compare some of the experimentally measured deposit profiles with the theoretical predictions for four values of Λ in figure 12. The agreement is seen to be very good and in particular the asymmetry predicted by the theory is accurately reflected by the data.

Using this simple model of the deposit it is straightforward to calculate numerically

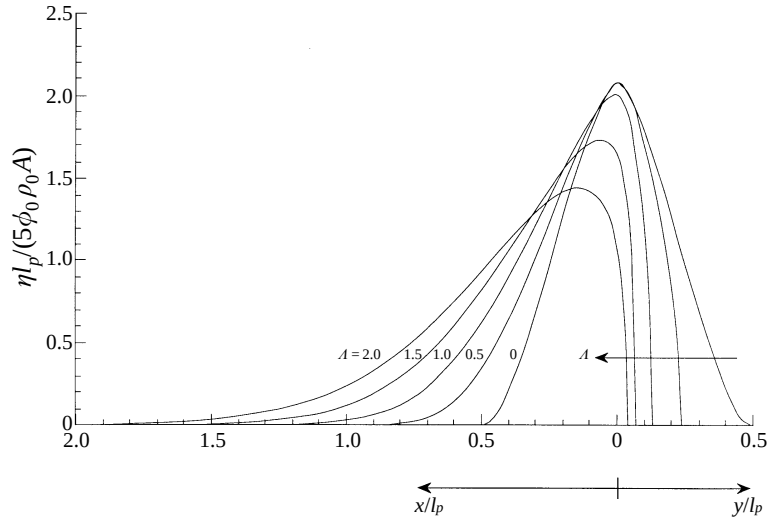

FIGURE 11. Non-dimensional deposit thickness as a function of position for a range of values of $\Lambda = 10UA/(V_s l_p^2)$.

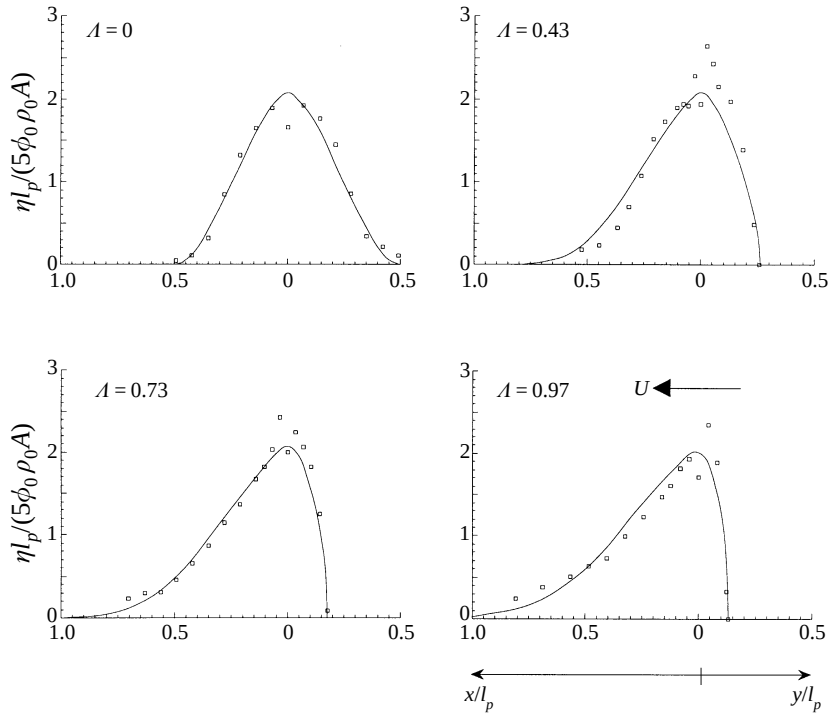

FIGURE 12. Plots of the experimentally measured deposit profiles and the theoretical predictions for four different values of $\Lambda = 10UA/(V_s l_p^2)$.

the maximum upstream distance, d_+, over which the current propagates, as a function of Λ. We present the results in figure 13 and find very good agreement between the theoretical curve and the experimental observations (except at $\Lambda = 0$, corresponding to zero flow, the situation in which the maximum upstream point is not as sharply

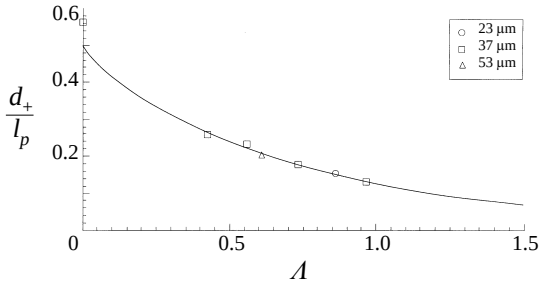

FIGURE 13. The maximum non-dimensional upstream distance d_+/l_p as a function of $\Lambda = 10UA/(V_s l_p^2)$. The calculation of the theoretical curve is described in § 3.2.

defined, as is seen from figure 11). From equations (3.12*c*) and (3.18) it is possible to calculate asymptotic representations of this maximum upstream distance in the regimes $\Lambda \ll 1$ and $\Lambda \gg 1$. We find, with the use of *Mathematica*, that

$$d_+/l_p = \tfrac{1}{2} + \left(\tfrac{1}{5}\log\Lambda - \tfrac{1}{8}\pi\right)\Lambda + \tfrac{1}{50}\Lambda^2 + O(\Lambda^3) \quad (\Lambda \ll 1), \tag{3.19a}$$

$$d_+/l_p = \frac{1}{6\Lambda^2} - \frac{1}{8\Lambda^7} + O(\Lambda^{-12}) \quad (\Lambda \gg 1). \tag{3.19b}$$

An approximate composite expansion derived from (3.19) which agrees well with the exact behaviour is given by

$$d_+/l_p = \frac{\tfrac{1}{2} + \left(\tfrac{1}{5}\log\Lambda - \tfrac{1}{8}\pi\right)\Lambda + \tfrac{1}{50}\Lambda^2}{1 + \tfrac{3}{25}\Lambda^4}. \tag{3.20}$$

4. Shallow-water analysis

4.1. *Model formulation*

Whereas in the preceding section we employed a 'box' model to describe the evolution of particle-driven gravity currents, we now derive a model of the flow that uses the more complete shallow-water equations. These exploit the low aspect ratio of the currents, defined as the ratio of the height to the length of the currents, and consider both temporal and spatial variations of the hydrodynamic properties of the flow. This approach is to be contrasted with 'box models', the derivation of which comes from horizontal integrals of the shallow-water equations (Hogg, Ungarish & Huppert 1998). It is to be expected that the use of the shallow-water equations would render more accurate results than the box model because use of the shallow-water equations is more rigorous. However, as demonstrated above, the box model approach provides an excellent general description of the flow up to an experimentally determined constant (§ 3.2) and also gives an analytical representation of the results.

As described in § 2, the gravity currents considered in this study were initiated by the sudden release of suspensions of relatively heavy silicon carbide particles. These were delivered into the ambient flow from an elevated reservoir, and during a very short initial period the suspension rapidly mixed with the ambient fluid. This mixing proceeded via turbulent motions which were both three-dimensional and unsteady. However, the gravity current soon propagated sufficiently far upstream and downstream that its length $l(t)$ was much greater than its height $h(x,t)$. Once this flow has been established, we may employ the 'shallow-water' description of the flow (as presented by Bonnecaze *et al.* 1993). In essence this approximation neglects

vertical accelerations which implies a hydrostatic pressure distribution. Furthermore, we assume that the dynamics of the flow are governed by a balance between buoyancy and inertial forces (and neglect effects of entrainment or viscosity). The dimensionless equations describing the conservation of mass and momentum are then given by (Bonnecaze *et al.* 1993)

$$\frac{\partial h}{\partial t} + \frac{\partial}{\partial x}(uh) = 0, \tag{4.1}$$

$$\frac{\partial}{\partial t}(uh) + \frac{\partial}{\partial x}\left(u^2 h + \tfrac{1}{2}\Phi h^2\right) = 0. \tag{4.2}$$

In these equations we have made the lengths, times and velocities dimensionless with respect to h_0, a characteristic initial height of the current after it has been released into the flow, $(h_0/g_0')^{1/2}$, where g_0' is the initial reduced gravity, and $(h_0 g_0')^{1/2}$, respectively. The volume fraction of particles is scaled by the initial volume fraction, ϕ_0. We have also assumed that the interstitial density of the suspension is the same as the ambient. (Sparks *et al.* 1992 and Bonnecaze *et al.* 1993 discuss effects due to the inclusion of differing interstitial and ambient fluid densities.)

On the assumptions that: the vertical mixing induced by the turbulence in the gravity current is sufficient to produce a vertically uniform distribution of particles; the particles sediment out of the current with velocity V_s; and the deposited particles are not re-entrained by the flow, the equation describing the evolution of the volume fraction of particles is given by (Bonnecaze *et al.* 1993)

$$\frac{\partial \Phi}{\partial t} + u\frac{\partial \Phi}{\partial x} = -\beta \Phi / h \tag{4.3}$$

(c.f. (1.10)) where $\beta = V_s/(h_0 g_0')^{1/2}$ is the dimensionless settling velocity.

The present analysis of two-dimensional currents in the presence of an ambient flow differs from previous analyses in the specification of the boundary conditions. While previous studies have considered only one moving front, in this scenario there are fronts which propagate both upstream and downstream. At the nose of a gravity current, the motions are unsteady and three-dimensional. Hence we do not expect the shallow-water approximation to be valid there. Instead, we invoke two frontal conditions which relate the difference between the velocity of the current at the nose and the mean velocity of the ambient felt by the current to the local shallow-water wave speed. This nose condition, as discussed in the Introduction, was developed by von Kármán (1940) and Benjamin (1968) for a quiescent ambient and has been experimentally studied by Huppert & Simpson (1980). The conditions, incorporating a steady mean flow in the ambient, may be expressed as

$$u(x_N, t) = Fr\,(\Phi(x_N, t)h(x_N, t))^{1/2} + U \tag{4.4a}$$

and

$$u(x_T, t) = -Fr\,(\Phi(x_T, t)h(x_T, t))^{1/2} + U \tag{4.4b}$$

(c.f. (3.2)) where x_N, $x_T = -y_N$ are the positions of the upstream and downstream propagating fronts and Fr is the Froude number. We use the experimentally determined Froude number condition (Huppert & Simpson 1980)

$$Fr = 1.19 \quad (0 \leqslant h(x_N, t)/H \leqslant 0.075) \tag{4.5a}$$

$$= 0.5(h(x_N, t)/H)^{-1/3} \quad (0.075 \leqslant h(x_N, t)/H). \tag{4.5b}$$

With zero ambient flow, this model of gravity current motion has been successfully

employed by a number of investigators (Rottman & Simpson 1983; Bonnecaze *et al.* 1993) and has been found to render good agreement with experimental observations. As in § 3 we do not account for any variation of the Froude number with the relative magnitude of the mean flow. For releases of a fixed volume of a suspension of particles these two boundary conditions are sufficient to enable the integration of the equations, subject to the specification of the initial conditions for the height, length, velocity and particle volume fraction of the current.

4.2. *Similarity solution*

In the case of vanishing particle settling velocity ($\beta = 0$), equations (4.1)–(4.3) describe the evolution of a gravity current with a fixed excess density over the ambient, such as for the compositional currents described in §§ 2.1, 3.1. In this limit, we may derive a similarity form of solution in an analogous manner to the solutions for gravity currents in a quiescent ambient with a single moving front. To derive this solution, we introduce the variables

$$\mathscr{L}(t) = x_N - x_T, \tag{4.6}$$

$$\mathscr{X}(t) = \tfrac{1}{2}(x_N + x_T), \tag{4.7}$$

$$\zeta = (x - \mathscr{X})/\mathscr{L}, \tag{4.8}$$

where $\mathscr{L}$ is the length of the current, $\mathscr{X}$ is the coordinate of the centroid and ζ is a suitable similarity variable. We denote the velocity of the flow, measured in a frame of reference which is moving with the centroid of the current, by $v = u - U$. Substituting (4.6)–(4.8) into (4.1) and (4.2), with $\Phi = 1$ corresponding to $\beta = 0$, we find the following equations govern the evolution of the current

$$\frac{\partial h}{\partial t} - \frac{y}{\mathscr{L}}\frac{\mathrm{d}\mathscr{L}}{\mathrm{d}t}\frac{\partial h}{\partial y} + \frac{1}{\mathscr{L}}\frac{\partial}{\partial y}(vh) = 0, \tag{4.9}$$

$$\frac{\partial v}{\partial t} - \frac{y}{\mathscr{L}}\frac{\mathrm{d}\mathscr{L}}{\mathrm{d}t}\frac{\partial v}{\partial y} + \frac{v}{\mathscr{L}}\frac{\partial v}{\partial y} + \frac{1}{\mathscr{L}}\frac{\partial h}{\partial y} = 0, \tag{4.10}$$

while the motion of the centroid is given by

$$\frac{\mathrm{d}\mathscr{X}}{\mathrm{d}t} = U. \tag{4.11}$$

The boundary conditions at the upstream and downstream fronts of the current indicate that

$$v(x_N, t) = Fr[h(x_N, t)]^{1/2}, \quad v(x_T, t) = -Fr[h(x_T, t)]^{1/2} \tag{4.12 a, b}$$

and

$$\frac{\mathrm{d}\mathscr{L}}{\mathrm{d}t} = v(x_N, t) - v(x_T, t), \tag{4.13}$$

while the conservation of the volume of the current requires that

$$\int_{-1/2}^{1/2} h\,\mathrm{d}\zeta = \mathscr{L}_0/\mathscr{L}, \tag{4.14}$$

where $\mathscr{L}_0 = A/h_0^2$ and A is the initial volume per unit width of the current. From these equations, a similarity solution may be calculated as

$$\mathscr{L} = (\Upsilon\mathscr{L}_0)^{1/3}t^{2/3}, \tag{4.15}$$

$$u = U + \tfrac{2}{3}(\Upsilon\mathscr{L}_0)^{1/3}t^{-1/3}\mathscr{U}(\zeta), \tag{4.16}$$

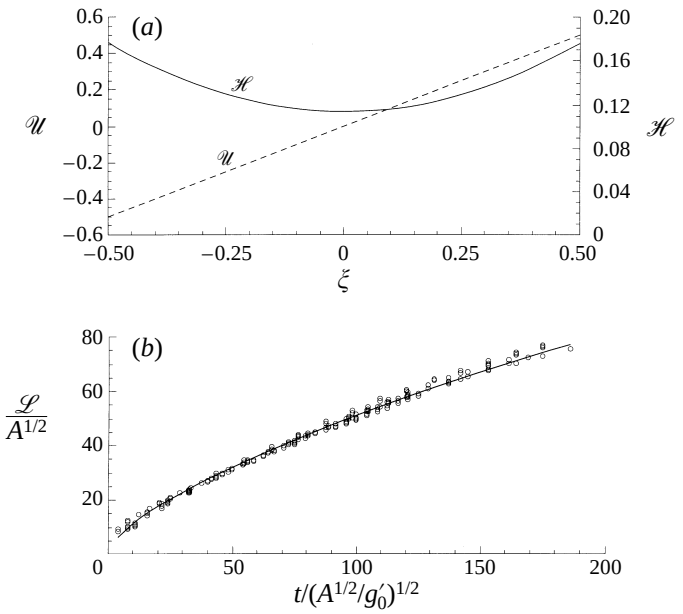

FIGURE 14. (*a*) The self-similar velocity $\mathscr{U}(\zeta)$ and height $\mathscr{H}(\zeta)$ for a homogeneous current of fixed volume with $Fr = 1.19$ at the nose. (*b*) The length of homogeneous gravity currents as a function of time. In this plot the length and time are non-dimensionalized with respect to $A^{1/2}$ and $(A^{1/4}/g_0'^{1/2})$ respectively. The data points are from the series of experiments described in § 2.2, while the theoretical curve arises from the similarity solution with $Fr = 1.1$.

$$h = \tfrac{4}{9}(\Upsilon \mathscr{L}_0)^{2/3} t^{-2/3} \mathscr{H}(\zeta), \tag{4.17}$$

where $\Upsilon = 54Fr^2/(6-Fr^2)$, $\mathscr{U}(\zeta) = \zeta$ and $\mathscr{H}(\zeta) = \zeta^2/4 + Fr^{-2}/4 - 1/16$. We plot this similarity form of solution in figure 14(*a*). Also we note that there is good agreement between the experimental observations and the temporal evolution of the length of the current if $Fr = 1.1$ which is slightly lower than the value proposed by Huppert & Simpson (1980).

The height of the current has been found to be an even function of the similarity variable ζ. In experiments, however, we observed a difference between the upstream and downstream propagating noses of the current. We suggest that this difference arises from the fluid motions in the layer above the current, as is further discussed below. We also note that this solution permits us to calculate the maximum upstream distance, y_{max}, over which a compositional gravity current will propagate. This is given by solving when $\mathrm{d}x_T/\mathrm{d}t = 0$ and hence, in dimensional terms, we find that

$$y_{max} = \frac{Fr^2 g' A}{(6 - Fr^2)U^2}. \tag{4.18}$$

This expression is to be compared with that calculated from the box model (§ 3.1). We note that the two differ only in the premultiplicative constant and that when the Froude number is order unity, this difference is relatively small.

4.3. *Numerical solution*

When the settling velocity of the particles is non-vanishing ($\beta \neq 0$), the form of similarity solution given above is no longer applicable. It is possible, however, for

times $t \ll \beta^{-3/5}$ to derive a perturbation expansion to the similarity solution (Hogg *et al.* 1998). In this paper, though, we perform a numerical integration of the equations, using the methods described by Bonnecaze *et al.* (1993). This approach formulates the equations into flux-conservative variables in a coordinate system which is scaled by the overall length of the current. In addition, for the present study, we consider the variables measured in a frame of reference that is moving with the centroid of the current. Therefore the equations are of a form similar to (4.9)–(4.13), except that the flux-conservative variables $q = uh$ and $\psi = u\Phi$ are used in place of u and Φ.

The numerical method employs an explicit scheme and uses outward propagating characteristics to provide additional boundary conditions to the Froude number conditions given above. The advantages of this scheme are that the formation and position of shocks need not be explicitly calculated. Shocks are expected to form in this system of equations as an internal bore separating a particle-free jet-like region at the centre of the current from a dense gravity current at the two fronts. This effect can be noted in the numerical results (see § 4.5). The drawback of this scheme is that a small timestep must be taken to ensure that the scheme remains stable. However run-times were only of order 10 minutes on an HP715/50 and so were not at all prohibitive.

4.4. *Two-layer flow*

It was noted by Rottman & Simpson (1983) and Bonnecaze *et al.* (1993) that for gravity currents propagating in relatively shallow depths of ambient fluid, it may be important to account for the motion of the upper layer. For currents within an otherwise quiescent ambient, the flow in the upper layer may be thought of as arising to satisfy mass conservation within the channel; effectively the forward propagating gravity current drives a return flow. For situations when there is an ambient flow with a given volume flux in the absence of the gravity current, we impose the condition that the sum of the volume fluxes of the gravity current and the upper layer must be constant (cf. Baines 1995). Using the suffix u to denote variables which are associated with the upper layer, we find that the dimensionless expressions of mass conservation within the two layers are given by

$$\frac{\partial h}{\partial t} + \frac{\partial}{\partial x}(uh) = 0, \tag{4.19}$$

$$\frac{\partial h_u}{\partial t} + \frac{\partial}{\partial x}(u_u h_u) = 0, \tag{4.20}$$

and the dimensionless balances of momentum are given by

$$\frac{\partial}{\partial t}(uh) + \frac{\partial}{\partial x}\left(u^2 h + \tfrac{1}{2}\Phi h^2\right) + h\frac{\partial p}{\partial x} = 0, \tag{4.21}$$

$$\frac{\partial}{\partial t}(u_u h_u) + \frac{\partial}{\partial x}\left(u_u^2 h_u\right) + h_u\frac{\partial p}{\partial x} = 0. \tag{4.22}$$

In these equations, we have denoted the interfacial pressure by p and have assumed that the particles are confined to the lower layer. Furthermore, we have ignored entrainment and the resulting drag between the two layers. In the context of the formation of saline wedges, these effects have been modelled by Arita & Jirka (1987*a*, *b*). We note that the drag force is only of a similar magnitude to the buoyancy and inertial forces during the latter stages of the flow of the current. Finally, since the particles are solely in the lower layer, we model the evolution of their volume fraction using (4.3).

We assume that the depth of the two layers is constant and so we may write

$$h_u(x,t) + h(x,t) = H, \tag{4.23}$$

where H is the total depth of the two layers. We note that the experiments were conducted for free-surface flows and so this condition is only an approximation, but a well-tested and largely valid one. Furthermore, the ambient has a constant volume flux Q in the absence of the gravity current and so from equations (4.19) and (4.20) we deduce that

$$h_u(x,t)u_u(x,t) + h(x,t)u(x,t) = Q. \tag{4.24}$$

We note that when the gravity current flows downstream its velocity exceeds that of the ambient (the upper layer). Therefore, the velocity of the upper layer must be reduced relative to the mean flow in the absence of a gravity current, in order to maintain this balance of volume fluxes. Conversely when the gravity current flows upstream the velocity of the upper layer must increase. In our experiments, by mounting the acoustic Doppler velocimeter to take velocity measurements in the upper layer we were able to observe this phenomenon quantitatively.

We use (4.22) to eliminate the interfacial pressure from the momentum equation of the lower layer (4.21) to find, with the aid of (4.23) and (4.24), that

$$\frac{\partial}{\partial t}(uh) + \left(\frac{H-h}{H}\right)\frac{\partial}{\partial x}\left(u^2h + \tfrac{1}{2}\Phi h^2\right) - \frac{h}{H}\frac{\partial}{\partial x}\left(\frac{(Q-hu)^2}{H-h}\right) = 0. \tag{4.25}$$

This approach is entirely equivalent to Bonnecaze *et al.* (1993); in their notation the dimensionless scales are defined such that $H = 1$ and there is no ambient flow ($Q = 0$). In this regime, equation (4.25) is the same as that presented by Bonnecaze *et al.* (1993) after the correction of a typographical mistake in the final term of their equation (24). We numerically integrate this system of equations using a similar numerical method to that described above. However, we note that this technique is only applicable when the ratio of the initial height of the current to the flow depth (h_0/H) is less than a critical value. (This value depends on the Froude number through the imposition of the boundary condition at the nose of the current. Rottman & Simpson (1983) demonstrate that the critical value is equal to $1/2$ when $Fr = \sqrt{2}$.) If the initial height exceeds this critical value then the flow is strongly influenced by 'upstream' conditions and this method using outward propagating characteristics fails. This effect was noted by Rottman & Simpson (1983) and they suggested that an internal hydraulic jump occurs, although their attempts to accommodate such a discontinuity into the formulation of their model were unsuccessful. Klemp, Rotunno & Skamarock (1994), however, developed a technique to model gravity current evolution when the initial depth exceeds the critical value. In this paper we restrict ourselves to cases when the ratio of the initial height to the flow depth is less than critical.

4.5. *Results*

In this subsection we review some of the results which may be generated from the numerical integration of this system of equations. The results presented here are not a complete set of those which may be produced from this model, but rather they reflect a number of the most significant characteristics. For each of the numerical calculations, the initial conditions were taken to be that the relatively heavy fluid was introduced into the ambient in a stationary state with unit aspect ratio. Such conditions are clearly not appropriate for direct comparison with the experimentally realized flows of §§ 2, 3 at early times. However, numerical experimentation indicates

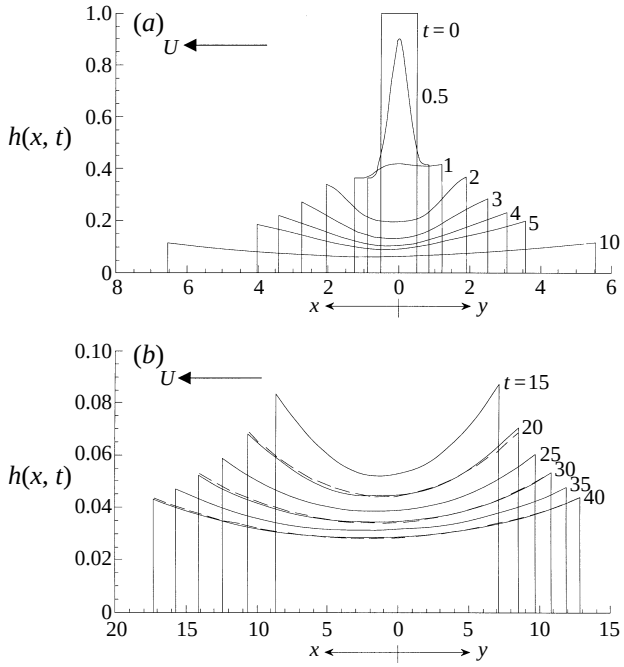

FIGURE 15. The numerically determined profiles of the height $h(x,t)$ of a collapsing homogeneous gravity current of fixed volume intruding into a deep ambient fluid moving with uniform velocity (single-layer model, mean flow $U = 0.1$). (*a*) The profiles at early times ($0 \leqslant t \leqslant 10$). (*b*) The profiles at later times ($15 \leqslant t \leqslant 40$). The dashed lines correspond to the similarity profile given by (4.17), where the length of the current has been fitted to the numerically determined length.

that the precise form of the initial conditions has relatively little effect on the long-time evolution of the numerical description of these gravity currents. Hence, we anticipate being able to model the motion adequately without a precise knowledge of the initial configuration.

First we consider the evolution of a homogeneous gravity current ($\beta = 0$) in the presence of a mean flow ($U = 0.1$) for both a single-layer and a two-layer model of the flow. We plot the height along the current at varying times after the initiation of the current in figures 15 and 16 and compare these with the similarity solution (§ 4.2). We note that the single-layer model evolves in a relatively symmetric manner about the centroid of the current, which itself is being advected downstream with velocity U. Furthermore, the similarity solution provides an accurate representation of the height of the current after approximately 10 non-dimensional units of time. In contrast, the height of the current in the two-layer model does not evolve symmetrically and the height of the downstream nose of the current is greater than the height of the upstream nose after an initial (short) period of adjustment. The asymmetry is such that the symmetric similarity solution never provides a particularly accurate representation of the height along the current.

This asymmetry has been noted before (Xu 1992; Xu & Moncrieff 1994). It may be rationalized by consideration of the distribution of the interfacial pressure which is given by

$$p = (u^2 h + u_u^2 h_u + \tfrac{1}{2}\Phi h^2)/H. \tag{4.26}$$

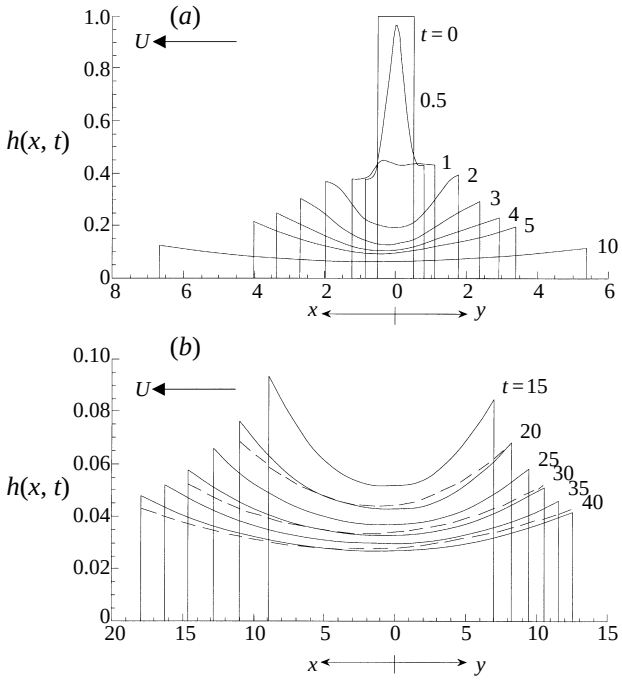

FIGURE 16. The numerically determined profiles of the height $h(x,t)$ of a collapsing homogeneous gravity current of fixed volume intruding into a shallow ambient fluid moving with uniform velocity (two-layer model, $h_0/H = 0.25$, mean flow $U = 0.1$). (*a*) The profiles at early times ($0 \leqslant t \leqslant 10$). (*b*) The profiles at later times ($15 \leqslant t \leqslant 40$). The dashed lines correspond to the similarity profile given by (4.17), where the length of the current has been fitted to the numerically determined length.

Eliminating the upper-layer variables, we find that

$$p = \frac{(Q^2 - 2hQu + u^2Hh)}{(H-h)} + \tfrac{1}{2}\Phi h^2. \tag{4.27}$$

Hence if the velocity of the current and the ambient are in the same direction ($Qu > 0$) then the pressure is lower than if the two velocities are in opposite directions ($Qu < 0$). Therefore the interfacial pressure acts to accelerate the fluid in the downstream direction and so relative to the mean flow the velocity of the upstream front is less than the downstream front. In turn this implies that the height of the downstream front is greater than the upstream front. We note that this difference, which is observed in experiments (§ 2), is entirely dependent upon the motion of the upper layer.

We now compare the box model with the numerical integration of the shallow-water equations. To this end we integrate the equations with various dimensionless settling velocities (β) until 95% of the particles have been deposited. (It is possible to integrate the equations until a greater proportion have settled out. However, the results are then more prone to significant numerical error, because the height of the current is very small. At such small heights, in any case, the governing equations should be altered to include viscous effects.) We re-scale the numerical results according to the box-model non-dimensionalization [lengths with respect to $h_0(10Fr/\beta)^{2/5}\mathscr{L}_0^{3/5}$ and times with respect to $5(g'_p\phi_0/h_0)^{-1/2}(10\beta^{3/2}Fr)^{-2/5}\mathscr{L}_0^{2/5}$] and plot the variation of the length and centroid of the current with time in figure 17. We find that the

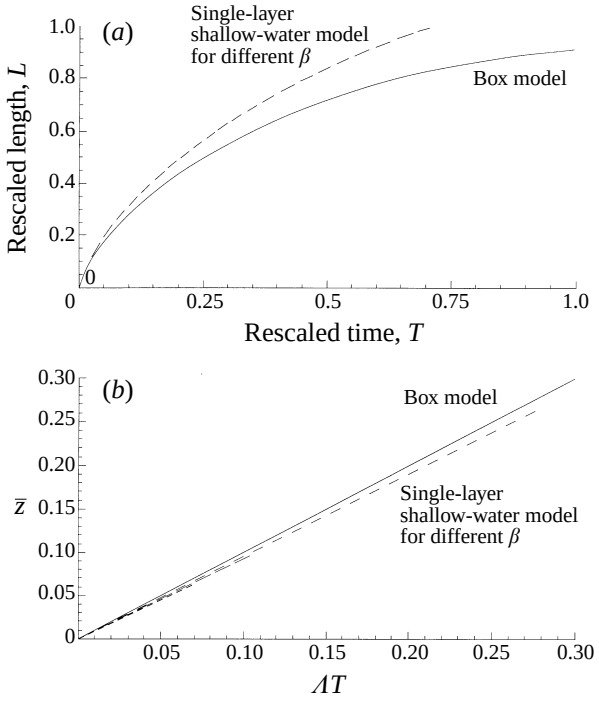

FIGURE 17. Comparison of the predicted evolution of (*a*) the length, and (*b*) the centroid of a particle-driven gravity current as a function of time for the box model and the single-layer shallow-water model. The length and time are non-dimensionalized according to the box-model scalings given by (3.14*a*, *c*). The numerical calculations are made with three settling velocities ($\beta = 0.01, 0.005$ and 0.001).

scaling collapses the numerical data. In figure 17(*a*), there are in fact three curves corresponding to numerical integrations of the shallow-water equations with different values of β. These curves, though, are indistinguishable under the box-model non-dimensionlization. This concurs with the findings of Bonnecaze *et al.* (1995) that under this non-dimensionalization different values of β yield only different initial conditions and the evolution becomes independent of these conditions after some initial time. However, the final length and the rate of growth in the length of the current are not identical with that predicted by the box model. This is not surprising since the box model is a considerable simplification of the shallow-water equations (Hogg *et al.* 1998). Our numerical experimentation over several orders of magnitude of β indicates that the box model under-predicts the runout length by a factor of approximately 1.2. We noted in § 3.2 that a knowledge of the initial volume of the particle-laden fluid was critical to permit the calculation of the runout length of the current. Also, for our experimental setup significant dilution occurs when the fluid is introduced into the ambient from the elevated reservoir. In § 3.2 we used a measured dilution of a factor of 20 and found good agreement with the box model. Here we note that had the dilution been 25% lower good agreement would have been found with the shallow-water analysis. We also note that the centroid of the current is indeed advected downstream at a constant velocity. We also compare the predictions of the distribution of the deposit arising from the passage of a particle-laden gravity current for both the box model and the numerical calculation (figure 18*a*, *b*). We find

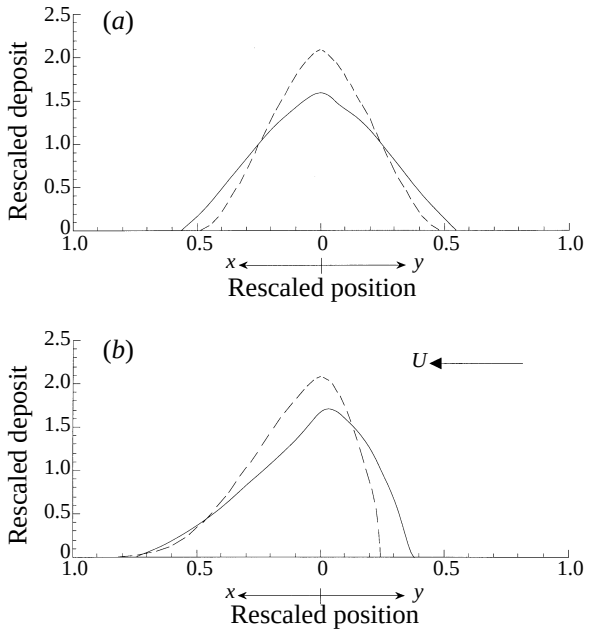

FIGURE 18. Comparison of the predictions of the distribution of the deposit between the box model (solid curve) and the single-layer shallow-water model (dashed curve) with non-dimensional settling velocity $\beta = 0.005$ for (*a*) a quiescent ambient fluid, and (*b*) a uniform ambient flow ($U = 0.2$). The deposit and position are non-dimensionalized according to the box-model scalings given by (3.16) and (3.14 *a*).

broad agreement between the two models, although the numerical integration predicts a slightly greater runout length of the current. Since the distribution of the deposit is over a slightly greater range, the maximum deposit is necessarily reduced.

Finally, we compare the numerical integration of the equations for particle-driven gravity currents in the single- and two-layer models. We plot the height and volume fraction of particles associated with the current along its length in figures 19 and 20. We note that in both cases the middle of the current, being thinner, becomes depleted in particles relative to the upstream and downstream propagating fronts. Furthermore, compared to homogeneous currents, the height of the front is increased. As with the homogeneous currents we note that while the single-layer model develops symmetrically about its centroid, the two-layer model develops significant asymmetry. This implies that the upstream propagating front is slower in the two-layer than in the single-layer model and vice versa for the downstream propagating front. Hence, although the total length of both currents increases similarly, the centroid moves downstream more rapidly in the two-layer model (figure 21) and the deposit is more heavily skewed towards the downstream direction (figure 22). Once again the difference between the two models of the current is due to the distribution of the interfacial pressure.

5. Discussion

5.1. *The nose condition in the presence of an ambient flow*

We noted in § 2 that although during the initial phase of the gravity current propagation the shape of the upstream and downstream flows were similar, an asymmetry

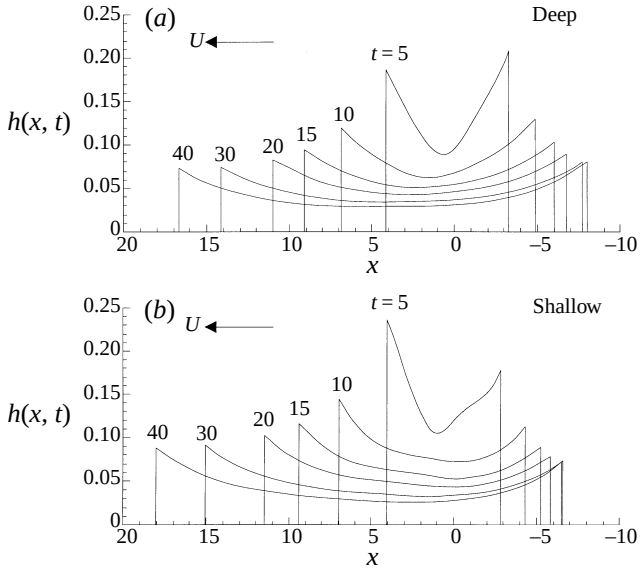

FIGURE 19. The numerically determined profiles of the height $h(x,t)$ of a collapsing particle-driven gravity current of fixed volume intruding into (*a*) a very deep ambient fluid (single-layer model) and (*b*) a relatively shallow ambient fluid (two-layer model, $h_0/H = 0.25$). In both cases, the non-dimensional settling velocity was given by $\beta = 0.005$, and initially the relatively heavy fluid was stationary and of unit volume with $h(x,t) = 1$. In this case the ambient fluid was moving uniformly with $U = 0.1$.

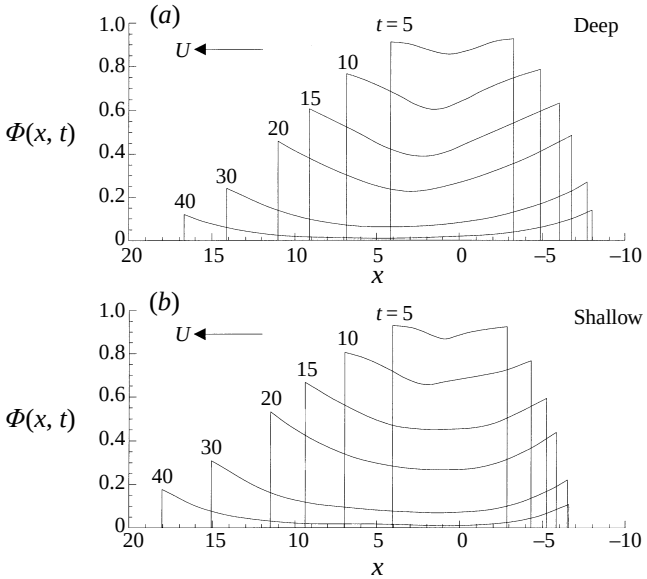

FIGURE 20. The numerically determined profiles of the volume fraction $\Phi(x,t)$ of a collapsing particle-driven gravity current of fixed volume intruding into (*a*) a very deep ambient fluid (single-layer model), and (*b*) a relatively shallow ambient fluid (two-layer model, $h_0/H = 0.25$). In both cases, the non-dimensional settling velocity was given by $\beta = 0.005$, and initially the relatively heavy fluid was stationary and of unit height and volume with $\Phi(x,t) = 1$. In this case the ambient fluid was moving uniformly with $U = 0.1$.

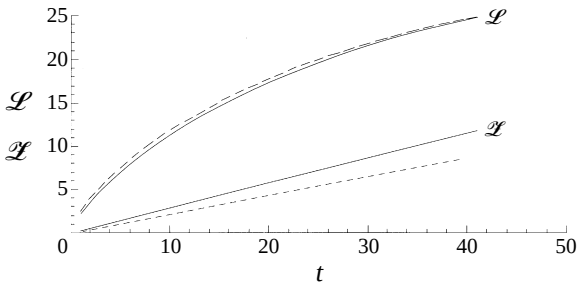

FIGURE 21. The length and centroid of a particle-driven gravity current of fixed volume as functions of time, intruding into a deep (dashed curve) and shallow (solid curve) ambient fluid. The settling velocity and the mean flow are given by $\beta = 0.005$ and $U = 0.1$ respectively. The depth of the shallow ambient is $h_0/H = 0.25$.

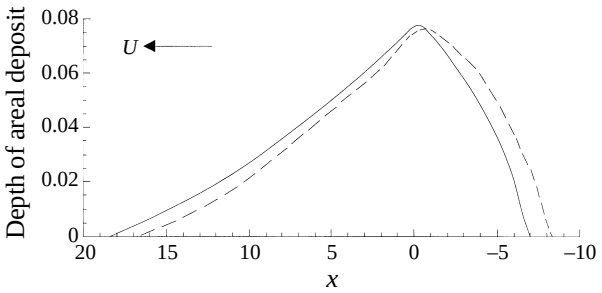

FIGURE 22. The numerically calculated deposit arising from the passage of a particle-driven gravity current of fixed volume, intruding into a deep (dashed curve) and shallow (solid curve) ambient fluid. The settling velocity and the mean flow are given by $\beta = 0.005$ and $U = 0.1$ respectively. The depth of the shallow ambient is $h_0/H = 0.25$.

soon developed. The current propagating upstream was considerably thinner than the downstream current and the elevation of the foremost part of the nose, relative to the overall height of the nose, was reduced. These observations have been noted before in studies of compositional gravity currents (Simpson & Britter 1980; Jirka & Arita 1987; Bühler, Wright & Kim 1991). Eventually the upstream current is arrested and adopts a wedge-like form before being stripped away by interfacial eddies. In the context of estuarine density wedges, a theory has been developed to model the shape of these wedge-like structures (Turner 1973). These models balance horizontal pressure gradients with the interfacial drag between the layers.

The detailed dynamics of the head of gravity currents have been the subject of some theoretical and experimental study (Britter & Simpson 1978; Simpson & Britter 1979), although most attention has focused on currents driven by a constant volume flux. The dynamics of these constant-flux currents are different from those of currents generated by the release of a fixed volume of fluid in that the head of the constant-flux currents are being continually replenished by fluid from the tail. Britter & Simpson (1978) suggest that this 'over-taking' velocity of the tail exceeds the velocity of the head by approximately 10%. In contrast no such overtaking is found for fixed-volume releases (Hallworth *et al.* 1996). Instead the head of these currents loses fluid to an almost stationary tail. It has been noted that the detailed flow structure of the head of a gravity current is extremely sensitive to anomalies in the flow relative to it. For currents generated by a fixed-flux release, both Jirka & Arita (1987) and Rottman,

Hunt & Mercer (1985) have formulated simple models of the flow in the region near the stagnation point at the foremost point of the head. Jirka & Arita (1987) conclude that the interface is flattened when the ambient flow is less than the velocity of the current and is steepened when the ambient exceeds the current. This is entirely in accord with our experimental observations. It also concurs with the observations of Simpson & Britter (1979).

In § 3, we found that the centroid of the gravity current was advected by a velocity of 0.6 times the mean flow. A similar factor has been reported by Simpson & Britter (1980) in the context of laboratory experiments with constant-flux currents and from a series of atmospheric measurements. They proposed a simple hydraulic model of the flow which may rationalize this observation. The model used principles of mass and momentum conservation, together with an empirically determined variation of the elevation of the foremost point of the nose as a function of the ratio of current velocity to the difference between the current and ambient velocities. We include a version of this analysis for constant-volume currents in the Appendix. Regrettably, there are as yet no experimental observations to validate fully this model and further experiments are required to understand the detailed dynamics.

5.2. *Applications*

Our results find immediate application in a number of different industrial situations. First, the upstream penetration of pollutants, either chemical or particulate, discharged into a stream or generated from a sedimented basement can be calculated. Second, the treatment of sewage and waste often consists of running suspended particulate matter sufficiently far down a channel for sedimentation of the solid waste to occur. Our results indicate the speed with which the separation takes place and the length of channel required.

Although the influence of an ambient flow on the propagation of a gravity current was considered more than fifty years ago, this paper presents the first definitive quantitative investigation of the problem. Nevertheless, extensions of the simplest situation considered in this paper immediately come to mind; and we plan to present investigations of at least some of them in the near future. These will include studies on the influences of: a fixed, or variable, flux to the input current, rather than the instantaneous release of a finite volume considered here; a distribution of particle sizes, rather than the monodisperse distribution assumed here; a relatively light interstitial fluid, rather than the case of equal densities of interstitial and ambient considered here; and the input into a moving ambient of fluid whose bulk density is less than that of the ambient.

We thank Stuart Lane for the generous loan of the acoustic Doppler velocimeter and Brian Dade, Ross Kerr, John Lister and Henry Pantin for helpful comments on an earlier draft. This research is partially supported by MAFF.

Appendix. Derivation of the nose condition

In this Appendix we propose a highly simplified analysis for the hydraulic properties of the flow around the head of a gravity current. This problem has received considerable earlier attention (Benjamin 1968; Britter & Simpson 1978; Simpson & Britter 1979, 1980; Klemp *et al.* 1994). The purpose here is to present a simplified version of the analysis developed by Simpson & Britter (1979) which is combined with an empirical observation of the height of the head of a gravity current origi-

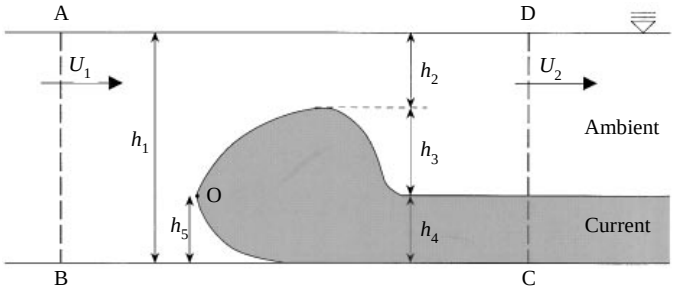

FIGURE 23. Schematic representation of a gravity current in a frame of reference which is moving with the velocity of the current at its head (U_0), showing the relative heights of the head ($h_3 + h_4$), its foremost point (h_5), the tail (h_4) and the ambient (h_1).

nating from the instantaneous release of a fixed volume (Hallworth *et al.* 1996). It is demonstrated that when a gravity current propagates through an ambient which has a mean flow, it is advected downstream by a proportion of the mean flow and that the Froude number at the head is reduced. We emphasize that the series of experiments reported in this paper do not provide a rigorous test of this simple model. Rather we include this analysis in order to consider more fully the influence of a mean flow on the hydrodynamics of the head of a gravity current.

The approach follows closely the work of Benjamin (1968) in that mass conservation and the Bernoulli equation are invoked. However, the analysis is extended to include the elevation of the foremost front of the gravity current (Simpson & Britter 1979). This foremost point is not at the boundary, as was assumed by Benjamin (1968), because of the action of viscous forces close to the boundary. We assume that the gravity current is in a quasi-steady state so that its acceleration may be neglected and within a control volume (which is specified below) the total momentum is conserved. Furthermore, entrainment into the head is ignored and we assume that there is a well-defined interface between the fluids of different density. This considerably simplifies the analysis of Britter & Simpson (1978). Finally, we assume that the combined depth of the two layers of fluid is constant. (This assumption was shown by Benjamin (1968) to be valid provided that the density difference is not too great.)

A schematic representation of the flow which is to be analysed is given in figure 23. We work in a frame of reference which is moving with the velocity of the gravity current at its head (U_0). In this frame the oncoming velocity is denoted by $U_1 = \overline{U} - U_0$. The total depth of the fluid is denoted by h_1, while the height of the tail of the gravity current is h_4. In this frame of reference the foremost point of the gravity current corresponds to a stagnation point, denoted by O in figure 23, which is elevated by a height h_5 above the boundary. Finally the total height of the head of the gravity current is given by $h_3 + h_4$. We consider, a control volume ABCD with the section AB and CD being sufficiently far from the head that the flow through these sections is horizontal and uniform. Applying mass continuity, we find that

$$h_1 U_1 = (h_1 - h_4) U_2. \tag{A 1}$$

Using Bernoulli's theorem on a streamline passing through the stagnation point at which the pressure is set equal to zero, we find that the pressure at B is given by

$$p_B = -\tfrac{1}{2}\rho_1 U_1^2 + \rho_1 g h_5 \tag{A 2}$$

and the pressure at C is given by

$$p_C = \rho_2 g h_5. \tag{A 3}$$

On each of the sections AB and CD we assume that the pressure adopts a hydrostatic distribution. Hence balancing the momentum fluxes across the two sections yields

$$\tfrac{1}{2}\rho_1 U_1^2 h_1 - \tfrac{1}{2}\rho_1 g h_1^2 + \rho_1 g h_5 h_1 = \rho_1 U_2 (h_1 - h_4)^2 - \tfrac{1}{2}\rho_1 g h_1^2 - \tfrac{1}{2}(\rho_2 - \rho_1) g h_4^2 \\ -(\rho_2 - \rho_1) g h_4 (h_1 - h_4) + \rho_2 g h_5 h_1. \tag{A 4}$$

Substituting for U_2 and writing $g' = \Delta\rho g/\rho$ and $\varphi = h_4/h_1$, we find that

$$\frac{U_1^2}{g' h_4} = \frac{(2-\varphi)(1-\varphi)}{(1+\varphi)} - \frac{2h_5(1-\varphi)}{h_4(1+\varphi)}. \tag{A 5}$$

The leading term of the right-hand side of this equation corresponds to that derived by Benjamin (1968), whereas the second term represents the influence of variations of the height of the foremost point. Simpson & Britter (1980) experimently studied this variation for fixed-flux compositional gravity currents. They proposed the empirical relationship that

$$\frac{h_5}{h_4} = -\Gamma \frac{U_0}{U_1}, \tag{A 6}$$

and found that $\Gamma(h_3 + h_4)/h_4 = 0.1$. For fixed-volume releases no equivalent measurements have been made. Furthermore, there has been no extensive research of the various dimensions of the head, although Hallworth *et al.* (1996) suggest that for two-dimensional gravity currents flowing over a rigid boundary $h_4 = (h_3 + h_4)/8$.

We may form an asymptotic solution to (A 5),(A 6) in the regime of $\Gamma \ll 1$ and of deep ambient fluid ($\varphi \ll 1$). This yields

$$U_0 = \left(2g' h_4\right)^{1/2} (1 - \varphi - \Gamma/2) + \overline{U}(1 - \Gamma/2) + O(\Gamma^2, \varphi^2, \Gamma\varphi). \tag{A 7}$$

Hence we observe that both the proportion of the mean flow experienced by the head of the gravity current and its effective Froude number are reduced by a factor of $(1 - \Gamma/2)$. Furthermore, if we use the experimental results of Hallworth *et al.* (1996) and Simpson & Britter (1980), even though the latter considered constant-flux gravity currents, we find that the head of the gravity current experiences a velocity only 0.6 times that of the mean flow – a result which was found from the experimental data in § 3. This result may be fortuitous because the model invoked here contains a number of simplifications and the relationship proposed in (A 6) is purely empirical. Nevertheless, we would highlight this as a future area of research. In particular, there is a need to understand the details of the complex dynamics around the head of the gravity current. To this end, future models of the motion should include effects due to three-dimensional flow and viscosity.

REFERENCES

Arita, M. & Jirka, G. H. 1987*a* Two-layer model of saline wedge I: entrainment and interfacial friction. *J. Hydr. Engng* **113**, 1229–1247.

Arita, M. & Jirka, G. H 1987*b* Two-layer model of saline wedge II: prediction of mean properties. *J. Hydr. Engng* **113**, 1249–1263.

Baines, P. G. 1995 *Topographic Effects in Stratified Flows*. Cambridge University Press, pp. 477.

Batchelor, G. K. 1970 Slender-body theory for particles of arbitrary cross-section in Stokes flow. *J. Fluid Mech.* **44**, 419–440.

Benjamin, T. B. 1968. Gravity currents and related phenomena. *J. Fluid Mech.* **31**, 209–248.

Bonnecaze, R. T., Hallworth, M. A., Huppert, H. E. & Lister, J. R. 1995 Axisymmetric particle-driven gravity currents. *J. Fluid Mech.* **294**, 93–121.

Bonnecaze, R. T., Huppert, H. E. & Lister, J. R. 1993 Particle-driven gravity currents. *J. Fluid Mech.* **250**, 339–369.

Bonnecaze, R. T., Huppert, H. E. & Lister, J. R. 1996 Patterns of sedimentation from polydispersed turbidity currents. *Proc. R. Soc. Lond.* A **452**, 2247–2261.

Britter, R. E & Simpson, J. E. 1978 Experiments on the dynamics of a gravity current head. *J. Fluid Mech.* **88**, 223–240.

Bühler, J., Wright, S. J & Kim, Y. 1991 Gravity currents advancing into co-flowing fluid. *J. Hydr. Res.* **29**, 243–257.

Chen, J. C. 1980 Studies on gravitational spreading currents. PhD thesis, California Institute of Technology.

Dade, W. B. & Huppert, H. E. 1994 Predicting the geometry of channelised deep-sea turbidites. *Geology* **22**, 645–648.

Hallworth, M. A., Huppert, H. E., Phillips, J. C. & Sparks, R. S. J. 1996 Entrainment into two-dimensional and axisymmetric turbulent gravity currents. *J. Fluid Mech.* **308**, 289–311.

Hogg, A. J., Ungarish, M & Huppert, H. E. 1998 Particle gravity currents: asymptotic solutions and box models. *J. Fluid Mech.* (to be submitted).

Huppert, H. E., Kerr, R. C., Lister, J. R. & Turner, J. S. 1991 Convection and particle entrainment driven by differential sedimentation. *J. Fluid Mech.* **226**, 349–369.

Huppert, H. E & Simpson, J. E. 1980 The slumping of gravity currents. *J. Fluid Mech.* **99**, 785–799.

Jirka, G. H & Arita, M. 1987 Density currents or density wedges: boundary-layer influence and control methods. *J. Fluid Mech.* **177**, 187–206.

Kármán, T. von 1940 The engineer grapples with nonlinear problems. *Bull. Am. Math. Soc.* **46**, 615–683.

Klemp, J. B., Rotunno, R. & Skamarock, W. C. 1994 On the dynamics of gravity currents in a channel. *J. Fluid Mech.* **269**, 169–198.

Lane, S. N, Biron, P. M., Bradbrook, K. F., Butler, J. B., Chandler, J. H, Crowell, M. D., McLelland, S. J., Richards, K. S. & Roy, A. G. 1997 Integrated three-dimensional measurements of river channel topography and flow processes using acoustic Doppler velocimetry. *Earth Surface Processes & Landforms (Technical & Software Bulletin)* (submitted).

Linden, P. F. & Simpson, J. E. 1990 Continuous two-dimensional releases from an elevated source. *J. Loss Prev. Process Ind.* **3**, 82–87.

Martin, D. & Nokes, R. 1988 Crystal settling in a vigorously convecting magma chamber. *Nature* **332**, 534–536.

Pantin, H. M. 1979 Interaction between velocity and effective density in turbidity flow: phase-plane analysis, with criteria for autosuspension. *Marine Geol.* **31**, 59–99.

Rottman, J. W., Hunt, J. C. R. & Mercer, A. 1985 The initial and gravity-spreading phases of heavy-gas dispersion: comparison of models with phase I data. *J. Hazardous Mater.* **11**, 261–279.

Rottman, J. W. & Simpson, J. E. 1983 Gravity currents produced by instantaneous releases of heavy fluid in a rectangular channel. *J. Fluid Mech.* **135**, 95–100.

Simpson, J. E. 1997 *Gravity Currents in the Environment and the Laboratory*. Cambridge University Press, pp. 244.

Simpson, J. E. & Britter, R. E. 1979 The dynamics of the head of a gravity current advancing over a horizontal surface. *J. Fluid Mech.* **94**, 477–495

Simpson, J. E. & Britter, R. E. 1980 A laboratory model of an atmospheric mesofront. *Q. J. R. Met. Soc.* **106**, 485–500.

Sparks, R. S. J., Bonnecaze, R. T., Huppert, H. E., Lister, J. R., Hallworth, M. A., Mader, H. & Phillips, J. C. 1993 Sediment-laden gravity currents with reversing buoyancy. *Earth Planetary Sci. Lett.* **114**, 243–257.

Turner J. S. 1973 *Buoyancy Effects in Fluids*. Cambridge University Press, pp. 367.

Xu, Q. 1992 Density currents in shear flows – a two fluid model. *J. Atmos. Sci.* **49**, 511–524.

Xu, Q. & Moncrieff, M. W. 1994 Density current circulations in shear flows. *J. Atmos. Sci.* **51**, 434–446.